Raman spectroscopy as an advanced structural nanoprobe for conjugated molecular semiconductors

Sebastian Wood,[1,2] Joseph Razzell Hollis,[2] Ji-Seon Kim[2]

[1] National Physical Laboratory, Hampton Road, Teddington, TW11 0LW, UK

[2] Department of Physics and Centre for Plastic Electronics, Blackett Laboratory, Imperial College London, London, SW7 2AZ, UK

Contents

Abstract

Raman spectroscopy has emerged as a powerful and important characterisation tool for probing molecular semiconducting materials. The useful optoelectronic properties of these materials arise from the delocalised π-electron density in the conjugated core of the molecule, which also results in large Raman scattering cross-sections and a strong coupling between its electronic states and vibrational modes. For this reason, Raman spectroscopy offers a unique insight into the properties of molecular semiconductors, including: chemical structure, molecular conformation, molecular orientation, and fundamental photo- and electro-chemical processes – all of which are critically important to the performance of a wide range of optical and electronic organic semiconductor devices. Experimentally, Raman spectroscopy is non-intrusive, non-destructive, and requires no special sample preparation, and so is suitable for a wide range of *in situ* measurements, which are particularly relevant to issues of thermal and photochemical stability. Here we review the development of the family of Raman spectroscopic techniques, which have been applied to the study of conjugated molecular semiconductors. We consider the suitability of each technique for particular circumstances, and the unique insights it can offer, with a particular focus on the significance of these measurements for the continuing development of stable, high performance organic electronic devices.

1. Introduction

The intention for this Review is that it provides a comprehensive (though not exhaustive) overview of the use of Raman spectroscopy for characterisation of conjugated molecular semiconductors. It is hoped that this might be of value, either as an introduction for the newcomer in the field or as a reference work for scientists already in this or a related field. As a result, it is anticipated that a typical reader will find some sections too specific and other sections too elementary. Sections 1 and 2 will be most valuable to those unfamiliar with organic semiconductors and Raman spectroscopy, respectively, whereas other readers might wish to skip ahead to Section 3 onwards, which describe and discuss the current state-of-the-art, capabilities, limitations, and future of the technique.

1.1. Conjugated Molecular Semiconductors

Whilst conjugated molecular semiconductors (both small molecules and polymers) were reported throughout the second half of the last century, widespread interest developed around the turn of the century when the breadth of applications and commercial potential of the technology became clear.[1–3] The key advantage of organic molecular semiconductors over traditional inorganic semiconductors is their processability. Organic semiconductor devices are usually based on thin film structures, which can be manufactured using many different methods including vacuum deposition (for small molecules and oligomers) and a wide range of solution-based printing and coating techniques (for soluble molecules and polymers). This flexibility results in a host of novel applications, since it is possible to deposit semiconducting materials onto almost any surface, or integrate them into other manufacturing processes in a way that is not possible with their inorganic counterparts. Additionally, printing and coating are readily scalable through roll-to-roll processes,

making the large-area, low-cost manufacture of electronics an exciting prospect that is fast becoming a reality.[4,5] In this Review we consider specifically conjugated molecules and polymers, in contrast to materials comprising carbon allotropes based on the graphene structure. The use of Raman spectroscopy for the characterisation of the latter class of materials is well-developed and comprehensively reviewed elsewhere.[6,7]

The optoelectronic properties of organic molecular semiconductors arise primarily from their chemical structures, and in particular the conjugated part of the molecule which is responsible for their semiconducting properties. The overlapping p-orbitals of adjacent atoms result in delocalisation of the π-electron density and give rise to π-bonding and π*-anti-bonding orbitals. As the conjugation length increases, these become quasi-continuous bands separated by an optical energy gap, as illustrated in Figure 1.[8,9] This electronic structure is analogous (though not identical) to the conduction and valence band structure of traditional semiconductors. The highest occupied molecular orbital (HOMO) and lowest unoccupied molecular orbital (LUMO) are typically separated by an optical energy gap in the range 1.5-3.0 eV resulting in strong optical activity in the visible range. The energy gap and optical activity can be manipulated by adjusting the chemical structure of the molecule or the solid state packing to control the optical absorption and emission spectra, making organic semiconductors especially suitable for light-emitting and light-harvesting applications. As a result, much ongoing research is directed towards the development of large-area lighting, displays, optical sensors, and solar cell applications.[10–13] The relationships between chemical structure and thin film optoelectronic properties are complex and not fully understood, so continued efforts are required to elucidate these mechanisms and to develop design rules for new materials.

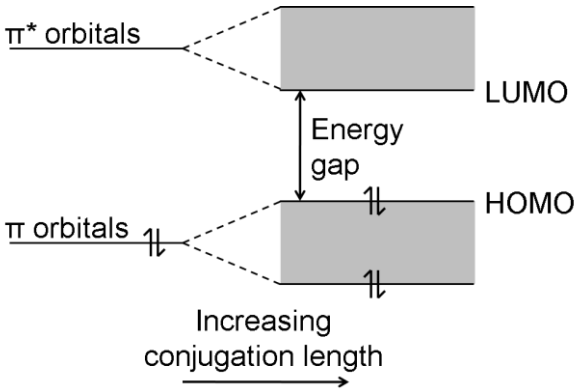

Figure 1. Diagram indicating π-orbital energy levels in a conjugated molecular semiconductor.

Charge transport in molecular semiconductors is distinct from the case of inorganic semiconductors because the dielectric constants of organic materials are generally low, and the π-electron density is not delocalised to the same extent. As a result, charge transport is usually described as 'hopping' where charge transfers from one molecule to another via overlapping π-systems, in contrast to the band transport through an inorganic semiconductor lattice.[3,9] Organic semiconductors (especially conjugated polymers) are relatively disordered materials in the solid state, so the charge carrier mobility is highly sensitive to the motif and quality of molecular packing. For most applications, and particularly for transistors, a high charge carrier mobility is desirable, so efforts are underway to optimise molecular structures and deposition processes in order to form highly ordered films of conjugated molecules with close π-π packing, where the co-facial π-systems overlap strongly.[14] In

general, the charge mobility in organic semiconductors is much lower than for inorganic semiconductors and is not expected to compete for high-speed electronic applications. However, several recent reports measure hole mobilities > 10 cm $V^{-1}s^{-1}$, which exceeds that of amorphous silicon, and demonstrate that these materials are suitable for many device applications including simple circuits, electronic paper, electronic skin, chemical and biological sensors. Ongoing work seeks to open up additional applications including near-field communications, and emissive displays, requiring new techniques for controlling the quality of molecular packing and charge transport.[12,13,15–21]

Organic photovoltaics combine the requirements for optimised light harvesting, with high charge carrier mobilities, but also introduce the challenge of separating localised excited states (Frenkel excitons) into separated charges (electron and hole polarons). The mechanism of this process is a subject of ongoing debate, but efficient exciton dissociation is usually achieved by blending two different organic semiconductors with different ionisation energies and electron affinities to make charge separation energetically favourable.[22,23] The efficiency of this process is strongly dependent on both the chemical structures of the materials, their respective molecular orbital energy levels and the morphology of the blend thin film. Due to the localisation of the Frenkel excitons, they have a limited diffusion length (5-10 nm) so only excitons generated within this range of a charge separating interface are able to be dissociated.[24–26] This requires nanoscale intermixing of the two materials, to maximise the interfacial area, whilst ordered molecular packing must also be maintained for efficient charge transport. These systems are particularly difficult to characterise and optimise since the performance depends not only on the properties of the constituents, but also on the interactions between them and the processing conditions used to form the blend film.

Over the past couple of decades, remarkable progress has been made in the performance of organic electronic devices, with record efficiencies and mobilities regularly reported. As a result, organic light-emitting diodes (OLEDs) have become a widely-used commercial technology. However, for other applications, significant progress is required to improve the operational lifetimes of organic semiconductor devices. This challenge is most pressing for photovoltaic applications, where products must endure prolonged exposure to outdoor conditions including exposure to air, water, direct sunlight, highly variable temperatures, mechanical stresses, and the electrical stress of continuous operation. Conjugated molecules typically have limited photochemical stability, particularly when exposed to UV light and in the presence of water and oxygen. They also tend to undergo morphological changes, especially at elevated temperatures.[27–29] In addition to the semiconductor itself, all the other components and the device as a whole must be stable. To date, lifetimes of up to 2 years have been achieved retaining 80 % of the initial efficiency, though not yet with the highest performing materials, and a target of 5 years is often suggested for a commercial product.[27]

In order to address the challenges highlighted here for the production of all types of high-performance, stable organic semiconductor devices, three overlapping research topics must be combined: 1) techniques for controlling material properties, 2) accurate measurement of device performance, and 3) detailed characterisation of nanomorphology and optoelectronic properties. This Review is particularly concerned with the third of these aspects, but many insights are dependent upon the first two.

1.2. Morphological and *In Situ* Characterisation

The properties of conjugated molecular semiconductors are strongly dependent on the thin film morphology. Morphology in this context refers not only to the structure of phase domains, but also to the molecular packing and intermixing in the solid state. Since most organic semiconductor samples comprise thin films with thicknesses in the range 10-500 nm, this structure is largely on the nanometre scale, though lateral domains can be much larger than this.[30,31]

Even in the simplest scenario, a thin film comprised of a single material, organic semiconductors can exhibit a wide range of morphologies from completely amorphous to crystalline depending on how the molecules pack together. Amorphousness can be desirable for optimised light emission or isotropic charge transport, and can be achieved using highly non-planar molecules, while crystals up to several centimetres long can be formed by highly ordered molecules and appropriate processing, such as zone-casting or shear-coating.[31–33] The majority of organic semiconductor films are semi-crystalline, falling between these two extremes with domains of relatively ordered material within a more disordered matrix.[34] Further complexity is introduced when two materials are blended together, which is typical for bulk heterojunction photovoltaics, but is sometimes considered for other applications too.[30,35] It is also increasingly common to incorporate additional components, for reasons such as the control of structural or mechanical properties, and the resulting morphologies are correspondingly more complex.[36–38]

In order to characterise the morphology of an organic semiconductor film, we are usually interested in knowing both the quantity and quality of ordered and disordered phases in the sample, *i.e.* how much of the material is ordered (disordered)? And how ordered (disordered) is this material? Molecular order in this case encompasses both the intramolecular conformational order (primarily, the planarity of the conjugated backbone) and the intermolecular packing (crystallinity), which are closely related properties. In reality the material occupies a continuous distribution between perfectly ordered and totally disordered, where the dimensions, shapes, interconnectivity, and molecular packing motifs and orientations of ordered domains also have an impact on the semiconductor properties.[34,39] For blended materials, both components need to be characterised and it is also important to consider the interactions between them. Most obviously, the degree of intermixing or phase separation is very important: for photovoltaics there is an optimum between complete intermixing, which compromises charge transport, and complete phase separation, which compromises charge generation.[30,40–42] One further morphological consideration is that the interfaces between different materials in a device may have distinct properties from the interior of the film, and this is particularly relevant to charge injection, separation, and extraction processes, which occur at these boundaries.[43,44]

Aside from the morphological complexity of organic semiconductor samples, an additional challenge for characterisation is posed by their sensitivity. Changes in the deposition conditions, device structure or dimensions, and post-fabrication treatment can significantly affect the sample properties and so it is desirable to perform any characterisation on complete devices. This is particularly important for correlating the morphological or optoelectronic properties of a sample with its device performance. *In situ* studies of this kind are also valuable for probing factors affecting the fundamental processes in devices such as charge generation, transport and recombination, where measurements are to be taken during device operation.[23] Similarly, degradation and

stability studies are most relevant if they are conducted on operational devices, since the relevant conditions and processes are difficult to reproduce otherwise.[45]

Many experimental techniques have been developed for the characterisation of organic semiconductors and a comprehensive comparison would lie beyond the scope of the present Review, but the broad categories are briefly discussed.[46,47] Electrical measurements provide the most direct insight into the semiconducting properties of conjugated molecule samples, and are obviously central to comparing the performances of devices using different materials, devices, or conditions. However, on their own, they offer very limited information about the morphology or fundamental properties of the sample. Conversely, X-ray scattering techniques can provide an effective probe for the morphology of organic semiconductors, but do not relate to the functional properties. X-ray diffraction is most suitable to the analysis of crystalline or semi-crystalline samples, since it is sensitive to material with periodic structures. Typically the signal from an organic thin film is very weak so an intense X-ray source at grazing incidence is required, which limits both the practicality of the technique and the spatial resolution achievable.[48,49] Nanometre spatial resolution measurements of organic samples can be obtained using atomic force microscopy or electron microscopy techniques, though both of these are restrictive in terms of sample preparation, are often limited to surface characterisation, and have limited sensitivity to chemical composition.[50,51] The most versatile class of characterisation techniques is optical spectroscopy, which is able to make use of all kinds of light-matter interactions including absorption, emission, and various types of scattering, to provide a direct probe for many optoelectronic properties of organic semiconductors, with additional sensitivity to the thin film morphology.[52,53] Among these techniques is Raman spectroscopy, which we now consider in more detail.

1.3. Applicability of Raman Spectroscopy

Raman spectroscopy is a form of vibrational spectroscopy, and so is inherently sensitive to the chemical structure of a sample. The Raman scattering process itself is based on the polarisability of the material, which, in the case of a conjugated molecule is very high as a result of the extended delocalisation of the π-electron system. This means that organic semiconductors typically display very high Raman scattering cross-sections (~10^{-24} cm^2 $molecule^{-1}$ sr^{-1}) and strong signals can be obtained easily.[54] The strong coupling between the electronic structure of a conjugated molecule and the chemical bonding also means that the intensity of Raman scattering and the frequency of the vibrational modes are sensitive to the molecular structure. As a result, Raman spectroscopy is able to detect, not only differences in the chemical structure of a material, but also variation in the molecular conformation and π-electron density distribution – particularly for the conjugated part of the molecule. The conformations of conjugated molecules relate closely to the molecular packing and so provide a probe for the overall degree of molecular order in a sample. In addition to this structural information, it is also possible to probe the properties of excited states and investigate their interactions using Raman spectroscopy. A large number of advanced techniques and variations have been developed, not all of which are considered in detail in this Review.

Experimentally, Raman spectroscopy requires only that there is optical access to the sample at the wavelength of the excitation beam, so is an ideal technique for *in situ* studies of complete device structures. Spatially resolved measurements and mapping are also readily achievable with diffraction

limited (sub-micrometre) resolution. Before considering the application of Raman spectroscopy to conjugated molecular semiconducting samples and what we can learn using these techniques, we offer a brief overview of the theoretical background.

2. Raman Scattering of Conjugated Molecules

2.1. Theory of Raman Scattering

Raman scattering is an inelastic light scattering process, where the difference in energy of the incident and scattered photon corresponds with the energy level separation between different states of the scatterer. In the simplest case, vibrational energy levels are probed using an optical excitation, whose photon energy is less than the optical energy gap, so the molecule is excited from the ground electronic state (S_0) to a virtual excited state (below the first excited electronic state, S_1) and relaxes back to the ground electronic state. Most scatterers relax back to their original vibrational state, such that the scattered photon has the same energy as the incident one, and this elastic scattering process is Rayleigh scattering. However, some scatterers relax to a different vibrational state, which is Raman scattering. When the final state has higher energy than the initial state, the scattered photon has less energy than the incident one, and this is described as Stokes scattering (in analogy to the Stokes shift observed in fluorescence). Relaxation to a lower-energy final state leads to a scattered photon with higher energy than the incident one, and is called anti-Stokes scattering. This form of scattering is typically weaker than Stokes scattering because their relative intensities depend on the initial populations of the excited and ground vibrational states respectively. These three scattering processes are compared in Figure 2.

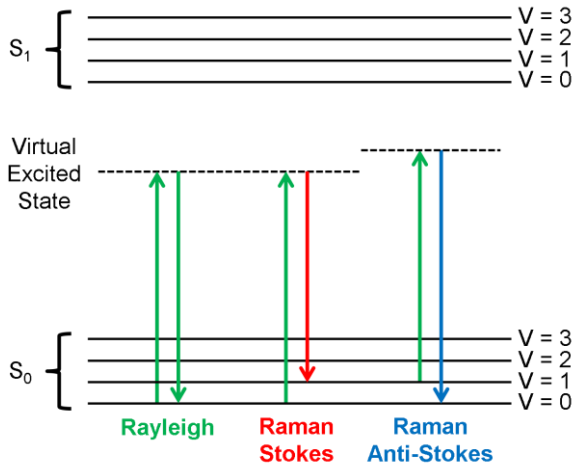

Figure 2. Diagram comparing energy level transitions for Rayleigh and Raman scattering with respect to the ground and first excited electronic states (S_0 and S_1), and vibrational energy levels with index V.

The difference in energy between the incident and scattered photons (known as the Raman shift) is directly related to the energy level spacing of the vibrational mode, and is usually quoted in units of cm^{-1}. A Raman spectrum consists of a series of scattering intensity peaks as a function of the Raman shift, and these peaks indicate the energies of different vibrational modes.

For conjugated molecules, visible excitation photon energies are often comparable to the optical energy gap of the sample, which meets the resonant excitation condition. In this regime the Raman cross-section is enhanced relative to the non-resonant case (see further discussion of this phenomenon below).

The theoretical detail of molecular Raman scattering is outside the scope of this Review, but a brief outline of the classical and quantum mechanical interpretations is given below, intended to provide sufficient background to understand the experimental results and interpretations reviewed here. An authoritative, and lucid account of the subject is to be found in the book by Long,[55] whilst other works offer very accessible introductions with a more experimental focus.[53,56,57]

2.1.1. Outline of Classical Theory

The classical description of Raman scattering considers the incident light as a time-varying electric field, *E(t)*, which acts to distort the electron cloud of the molecule. This creates an induced dipole moment, μ, that depends on the polarisability, α, of the molecule (how easily the electron cloud is distorted).[53,58] In fact, the polarisability of the molecule varies as the molecule vibrates, and the collective motion of a vibrational normal mode can be described using a vibrational coordinate, Q:

$$\mu(t) = \alpha E(t), \text{ where } \alpha = \alpha_0 + \left(\frac{\partial \alpha}{\partial Q}\right)_0 Q + \cdots. \quad (1)$$

Here, α_0 is the polarisability at equilibrium, and $(\partial\alpha/\partial Q)_0$ is the derivative of polarisability with respect to the vibrational motion, evaluated at the equilibrium position. We can consider the optical excitation as a sinusoidal electric field with frequency, ω_0, and amplitude, E_0, while the time dependence of the vibrational coordinate, *Q(t)*, is treated as a simple harmonic oscillation with amplitude, Q_0, and frequency, ω_v , *i.e.*:

$$E(t) = E_0 \cos(\omega_0 t), \quad \text{and} \quad Q(t) = Q_0 \cos(\omega_v t). \quad (2)$$

Combining these equations results in:

$$\mu(t) = E_0 \alpha_0 cos(\omega_0 t) + \frac{E_0}{2}\left(\frac{\partial \alpha}{\partial Q}\right)_0 \{\cos[(\omega_0 + \omega_v)t] + cos[(\omega_0 - \omega_v)t]\}. \quad (3)$$

This expression shows that the induced dipole oscillation has three components with frequencies ω_0, $(\omega_0 + \omega_v)$, and $(\omega_0 - \omega_v)$ corresponding to Rayleigh, anti-Stokes Raman, and Stokes Raman scattering respectively. This simple model is equivalent to describing Raman scattering as Rayleigh scattering with its amplitude modulated by a molecular vibration. Typically, molecules have multiple vibrational modes so *Q* becomes Q_j (for *j* vibrational modes) and additional terms are needed in the polarisability to include all of the modes. Any given mode will only be Raman-active if $(\partial\alpha/\partial Q)_0 \neq 0$ *i.e.* if the vibrational mode results in a change in molecular polarisability at the equilibrium position.

There are several short-comings to this classical description. Firstly, it predicts equal intensities of Stokes and anti-Stokes scattering (usually Stokes scattering is much stronger). Secondly, no selection rules are predicted (overtones are not usually observed in non-resonant Raman spectra). Thirdly, this description started with a vibrating molecule (Raman scattering is observed for molecules which start in a vibrational ground state). All of these problems are resolved by using a quantum mechanical description where the states and transitions are properly represented.

2.1.2. Quantum Mechanical Interpretation

Quantum mechanically, Raman scattering is described in terms of transitions between states, as shown above in Figure 2.[53,55,56,59] The virtual excited state is a very short-lived 'state' representing the molecule in its equilibrium nuclear geometry, but with a distorted electron cloud. The electronic distortion itself depends on how much energy has been given to the molecule, and

hence is determined by the wavelength of the incident photon. This interaction is described by the quantum mechanical expression for molecular polarisability, known as the Kramer-Heisenberg-Dirac expression:

$$\left(\alpha_{\rho\sigma}\right)_{fi} = \frac{1}{\hbar}\sum_{r\neq i,f}\left[\frac{\langle f|\hat{p}_\rho|r\rangle\langle r|\hat{p}_\sigma|i\rangle}{\omega_{ri}-\omega_0-j\Gamma_r} + \frac{\langle f|\hat{p}_\sigma|r\rangle\langle r|\hat{p}_\rho|i\rangle}{\omega_{rf}+\omega_0+j\Gamma_r}\right] \qquad (4)$$

where *i,r,* and *f* represent the initial, virtual excited, and final states respectively; $(\alpha_{\rho\sigma})_{fi}$ are components of the general transition polarisability, $(\alpha)_{fi}$, for the Raman transition from *i* to *f* where ρ and σ are the incident and scattered polarisation directions; $\hat{p}_\rho$ and $\hat{p}_\sigma$ are the ρ and σ components of the electric dipole moment operator; ω_0 is the frequency of the incident photon; ω_{ri}, and ω_{rf} are the frequency differences between states *r* and *i*, and between states *r* and *f* respectively; *j* here is the imaginary unit; and Γ_r is the natural half-width of state *r*.

This sum is dominated by the first term and values of *r* that give ω_{ri} and ω_0 similar magnitudes so the second term can be neglected. A further simplification arises from the Born-Oppenheimer approximation: for vibrational Raman scattering, we consider only the electronic, θ, and vibrational, Φ, parts of the wavefunction. Since the electronic wavefunction depends on both the nuclear and electronic coordinates, $\theta(R_N,R_e)$, while the vibrational term depends only on nuclear coordinates, $\Phi(R_N)$, the electric dipole operator only acts on the electronic part so we can rewrite the integral:

$$\langle r|\hat{p}_\sigma|i\rangle = \langle\theta_r|\hat{p}_\sigma|\theta_i\rangle\langle\Phi_r|\Phi_i\rangle = M_{ri}\langle\Phi_r|\Phi_i\rangle, \qquad (5)$$

where M_{ri} is the corresponding transition moment.

In the Raman scattering process, the vibrational state of the molecule changes but no significant nuclear movement occurs on this fast time scale so the dependence of the transition moment on the nuclear coordinates can be approximated by:

$$M_{ri}(R_N) = M_{ri}(R_0) + \left(\frac{\partial M_{ri}}{\partial R_E}\right)_{R_0} R_E + \cdots, \qquad (6)$$

where R_0 represents the equilibrium nuclear coordinates and R_E represents a displacement in the nuclear coordinates.

Using these expressions and simplifications and the approximation $M_{ri} = M_{fr}$, we can write:

$$\left(\alpha_{\rho\sigma}\right)_{fi} \approx \frac{1}{\hbar}M_{ri}^2(R_0)\sum_{r\neq i,f}\frac{\left\langle\Phi_{R_f}\middle|\Phi_{R_r}\right\rangle\left\langle\Phi_{R_r}\middle|\Phi_{R_i}\right\rangle}{\omega_{ri}-\omega_0-j\Gamma_r} \quad (A\ term) \qquad (7)$$

$$+\frac{1}{\hbar}M_{ri}(R_0)M'_{ri}(R_0)\sum_{r\neq i,f}\frac{\left\langle\Phi_{R_f}\middle|R_E\middle|\Phi_{R_r}\right\rangle\left\langle\Phi_{R_r}\middle|\Phi_{R_i}\right\rangle + \left\langle\Phi_{R_f}\middle|\Phi_{R_r}\right\rangle\left\langle\Phi_{R_r}\middle|R_E\middle|\Phi_{R_i}\right\rangle}{\omega_{ri}-\omega_0-j\Gamma_r} \quad (B\ term)$$

where $M' = (\partial M/\partial R_E)_{R_0}$.

The A and B terms are the dominant terms but two further terms (C and D) related to vibronic coupling between various different electronic states are significant in some cases.[55] The A term is

sometimes called the Franck-Condon term, and the B term is also known as the Herzberg-Teller term.

The total scattering intensity, I_R, of a Raman transition (from state *i* to state *f*) for a single molecule is given by:

$$I_R = \frac{8\pi\omega_s^4 I_0}{9c^4} \sum_{\rho\sigma} \left| (\alpha_{\rho\sigma})_{fi} \right|^2 \qquad (8)$$

where I_0 is the incident laser intensity and ω_s is the frequency of the Raman scattered light.

Experimentally, the relationship between incident and scattered intensities is expressed using a Raman scattering cross-section, σ_j, for each vibrational mode:

$$I_R = I_0 \sigma_j D dz \qquad (9)$$

Where *D* is the number density of scatterers and *dz* is the excitation path length (or depth of field).

This cross-section includes light scattered in all directions, whereas practical measurements collect only a portion of the total scattered light according to the solid angle covered by the detector, Ω. For this reason, the differential Raman cross-section, β_j, is expressed in units of m^2 $molecule^{-1}$ sr^{-1} and is defined by:

$$\beta_j = \frac{d\sigma_j}{d\Omega}. \qquad (10)$$

This β_j value is proportional to the integrated area of the peak in a measured Raman spectrum corresponding to vibrational mode *j*.

Non-Resonant Raman Scattering

In the non-resonant case, where the transition dipole moment, M_{ri}, is small and the denominator of Equation 7 shows minimal variation for different *r* values, the summation in the A term over all *r* reduces it to the overlap of the *i* and *f* vibrational wavefunctions, due to the completeness property. These states are orthogonal unless *i* and *f* are equal (*i.e.* Rayleigh scattering), and so this term is zero.

The intensity of Raman scattering in this case is dominated by the B term. This term is subject to a quantum mechanical selection rule that its value is only non-zero when the initial and final vibrational states differ by one quantum of energy, meaning that overtones are forbidden.

Resonant Raman Scattering

Under resonant conditions, the denominator in term A will be very small when *r* corresponds to a real electronic excited state of the molecule, such that the sum is dominated by a single resonant term. However, the term is still dependent on the vibrational overlap integrals. If two vibrational wavefunctions are orthogonal, their overlap integral will be zero, and this will be the case if the vibrational modes have the same energy levels in the ground and excited states of the molecule. Non-orthogonality arises when the excited state potential energy surface of the molecule is different from that of the ground state, either having a different shape (*i.e.* ground and excited state vibrational modes have different frequencies), or a displacement of the potential energy minimum along the vibrational coordinate, ΔQ_j, (*i.e.* equilibrium geometry of the molecule is different in ground and excited states), see Figure 3**Error! Reference source not found.**. The latter case is usually

more significant in conjugated molecules. Overtones are not forbidden in this term and so are frequently observed, especially when ΔQ_j is large. Because of this sensitivity to the change in equilibrium coordinate, ΔQ_j, resonant Raman spectroscopy can be used to probe the excited state geometry of a molecule.[60]

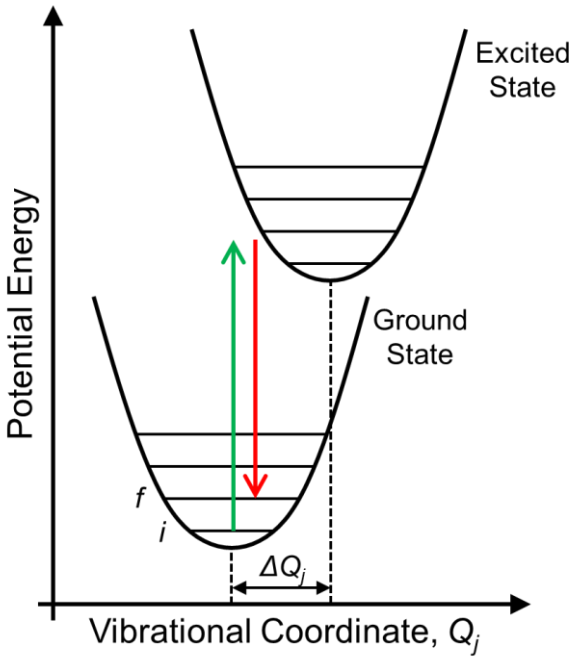

Figure 3. Resonant Raman transition showing potential energy surfaces for vibrational mode j in the ground and excited electronic states of the molecule.

Term B may also be significant in resonant Raman scattering, since the resonant effect in the denominator is also present, however its magnitude is generally low compared with that of the A term since $M'M < M^2$, so term A is dominant. The B term resonant enhancement relates to the case where there are two electronic transitions with similar energy and can result in scattering from forbidden transitions.

2.1.3. Raman Scattering of Conjugated Molecules

The particular suitability of Raman spectroscopy for studying conjugated molecules has been recognised for several decades, most notably by Zerbi and co-workers.[61,62] In addition to the relative ease of measuring Raman spectra from these materials on account of their large Raman scattering cross-sections, these spectra also show strong sensitivity to subtle changes in the molecular properties and conditions. This sensitivity arises from the interconnection between the distribution of electron density in the π-system and the positions of the nuclei in the molecule, which is often referred to as electron-phonon coupling. Usually, the term 'phonon' is reserved for vibrational normal modes in lattice structures, but is sometimes borrowed to describe vibrational normal modes in molecular materials.

Typically, Raman spectra measured for highly conjugated molecules are dominated by a small number of peaks in the region 1300 cm^{-1} to 1700 cm^{-1}, which correspond with stretching modes of the carbon-carbon bonds in the conjugated part of the molecule. Raman dispersion is also commonly observed, where the energies of some vibrational peaks shift as a function of the excitation wavelength or the effective conjugation length.[61] Several models have been devised to describe these effects, including the conjugation length model (CLM),[63,64] amplitude mode model (AMM),[65,66] and effective conjugation coordinate model (ECCM).[67,68] The ECCM has the greatest explanatory power, and is built on the hypothesis that a single dipole-allowed electronic state is responsible for the observed Raman scattering, even under non-resonant conditions. The excited state of relevance is assumed to be the first excited state, and the transition from the ground state to this excited state is characteristically described as a stretch of the C=C bonds and a contraction of the C-C bonds along the conjugated structure. The displacements of the nuclei corresponding with this transition can be described by an internal coordinate, *Я*. This model has been applied to several conjugated polymers, and Figure 4 illustrates how *Я* is defined in several cases.[69,70]

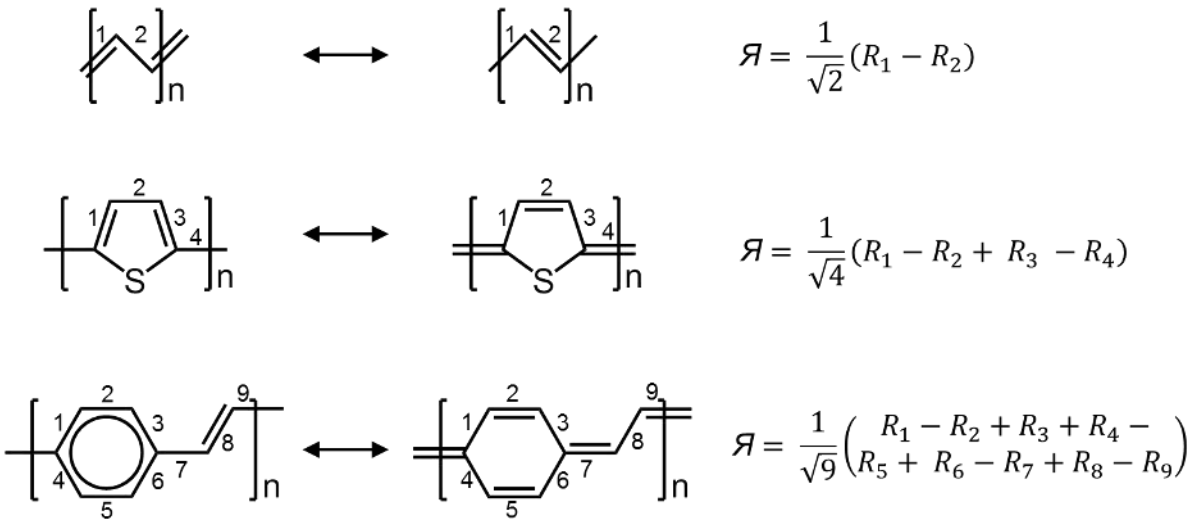

Figure 4. Diagram showing definitions of Я coordinates for (top to bottom) polyacetylene, polythiophene, and polyparaphenylenevinylene.[69,70]

The *Я* coordinate describes the direction along which the electron-phonon coupling is most effective, and so the strongest peaks are measured for those Raman-active normal vibrational modes which

have strong contributions along *Я*. For conjugated polymers, these are usually the C-C and C=C collective stretching modes along the conjugated backbone. Raman dispersion in this model is described by the effective force constant, $F_Я$, which depends on the effective conjugation length and increased conjugation leads to lower $F_Я$ values. This effect is neatly demonstrated by considering the experimental Raman spectra of a series of polyacetylenes with different conjugation lengths (Figure 5), which show a softening of the C-C mode and particularly the C=C mode (labelled R4 in the figure) with increasing conjugation.

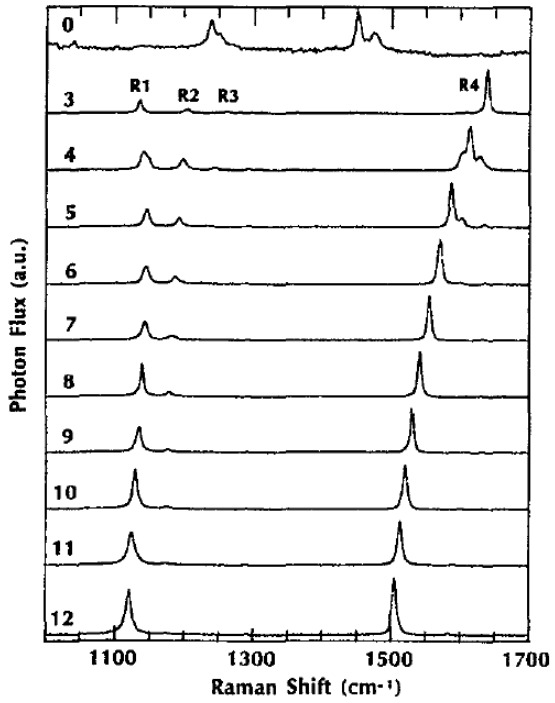

Figure 5. Raman scattering spectra of t*-butyl capped polyacetylenes with 0, and 3 to 12 double bonds. Main Raman peaks labelled R1 to R4.* [71] *Reprinted from H.E. Shaffer et al., Journal of Chemical Physics, 94, 4161, (1991), with the permission of AIP Publishing.*

For several different conjugated molecules, the ECCM has been found to provide a valuable basis for the interpretation of experimental Raman spectra, since large molecules are expected to have many vibrational normal modes, but typical spectra show a relatively small number of peaks. The ECCM identifies the small number of strongly Raman active modes as those with strong components along the *Я* coordinate, *i.e.* symmetric stretching modes of the conjugated part of the molecule. Specific identification of modes can be achieved by comparing spectra with those of other, similar molecules or tables for particular bonds.[72]

The ECCM was developed with respect to relatively simple conjugated molecular structures, and it remains to be seen whether it is valid for more complex structures, such as donor-acceptor copolymers, which are of particular contemporary interest. The optoelectronic properties of these materials often show significant contributions from more than one excited state and so it is not clear that their properties can be described in terms of a single *Я* coordinate.

Another tool for interpreting Raman spectra is density functional theory (DFT) calculations, which generally give accurate values for vibrational mode energies of conjugated molecules (using appropriate methods and scaling factors).[73,74] The accurate prediction of mode energies means that DFT can be used to identify the specific natures of various vibrational modes, but the calculated Raman activities are not reliable, and do not consider the couplings to particular electronic excited states. As a result, DFT does not accommodate resonant effects or the ECCM, and so tends to predict more Raman peaks than are experimentally observed, making it difficult to assign the peaks using DFT alone. To some extent this limitation can be addressed using time-dependent DFT, which can give a better estimate of Raman intensities.[60,75]

2.1.4. Polarisation Dependence of Raman Scattering

The polarisability of a molecule for a transition is generally not isotropic and is represented by a second-rank tensor. As a result, the Raman scattering itself is anisotropic too and can be described using Raman tensors, $\boldsymbol{R_j}$, where *j* is the index of the Raman-active vibrational mode. The form of the Raman tensor can, therefore, be probed by measuring the dependence of the Raman scattering intensity on the polarisation of the incident and scattered light. The relationship is expressed by:

$$I_s \propto \left|\boldsymbol{e_s} \cdot \boldsymbol{R_j} \cdot \boldsymbol{e_i}\right|^2 \qquad (11)$$

where, I_s is the measured intensity of Raman scattering, $\boldsymbol{R_j}$ is the Raman tensor of mode *j* for the molecule, $\boldsymbol{e_i}$ is the electric field vectors of the incident light, and $\boldsymbol{e_s}$ is the electric field vector sampled by the instrument.

Much of the literature concerned with the polarisation of Raman scattering assumes an isotropic sample with freely rotating molecules, in which case the measured property is the depolarisation ratio, $\rho = I_\perp / I_\parallel$, where $I_\perp$ and $I_\parallel$ are the scattering intensities with the polariser and analyser oriented perpendicular or parallel to one another, respectively.[55] However, since most organic semiconductors have some degree of anisotropy in the solid state, molecular orientations must also be considered. This is usually achieved using Cartesian coordinates to describe the measurement and sample system and describing the scattering process using Jones calculus.[76] The orientation of the molecule itself can be represented in a number of different ways, and there is no clear consensus. Euler angles are a common choice, though it is important to identify which of the many possible conventions is being used in any particular situation, and alternative representations are equally valid.[77]

2.2. Experimental Raman Spectroscopy

One of the appealing features of Raman spectroscopy as a characterisation technique is the ease and speed with which measurements can be taken using commercially available equipment. However, there are a number of caveats and complexities to be considered. These experimental considerations are discussed in depth by McCreery,[78] and this Review highlights just a few issues, which are particularly relevant to conjugated molecule samples.

2.2.1. Non-Resonant Raman Spectroscopy

It has been mentioned already that the only requirement for samples is that there is optical access for the incident and scattered light. However, there are several other factors that affect the measurement and the quality of the data. The primary challenge for Raman spectroscopy is to separate the Raman scattered light from the much more intense Rayleigh scattering, and other light

detected by the spectrometer. The Rayleigh scattering is removed using a wavelength specific filter, and these are very effective in most cases, though problems can arise if the Raman peaks of interest have low wavenumbers (< 50 cm^{-1}) such that the Raman and Rayleigh scattered light have very similar wavelengths. Other contributions to the background of the Raman spectrum arise from a variety of sources (including, but not limited to fluorescence) and are often described collectively as the 'fluorescence background' – typically this background is removed from the spectrum by simply fitting a smooth curve and subtracting it. Even under non-resonant excitation conditions, the background can mask the Raman spectrum, and if there are peaks or other features in the background spectrum, the subtraction also becomes difficult. The optical properties of the sample holder, substrate or solvent should also be considered, since they must be transparent and non-emissive at the relevant wavelengths. If they are Raman active, care is needed to distinguish their Raman scattering from that of the sample itself. These considerations dictate the design of the sample holder, but permit a great degree of freedom for *in situ* measurements, where the Raman spectrum of a sample can be measured under various different conditions such as temperature, pressure, and atmospheric control.

From a metrological perspective, Raman spectroscopy is a particularly challenging technique. Accurate measurements of wavenumber for Raman-active vibrational modes are relatively simple, and reference samples with well-known scattering peaks, such as silicon and diamond can be used for spectral calibration. However, robust measurements of Raman scattering cross-sections require highly specialised equipment.[78] The light-collection efficiency and instrument response function of the spectrometer must be considered, since the scattering cross-section considers light scattered in all directions, and a real instrument collects only the portion scattered in a particular direction. This factor depends on the geometry of the measurement, and is very difficult to control. For this reason, published work on conjugated molecular semiconductors using Raman spectroscopy tends to rely on comparisons between spectra measured under (approximately) constant experimental conditions, rather than absolute scattering cross-sections.

2.2.2. Resonant Raman Spectroscopy

The instrumentation and experimental requirements of resonant Raman spectroscopy are the same as for the non-resonant case described above, but with a few additional considerations. Resonant excitation of a sample results in a strong increase in the intensity of the Raman scattering (by up to 4-5 orders of magnitude), but also means that optical absorption is a significant effect resulting in a correspondingly high level of fluorescence emission. Since many conjugated molecules are highly emissive (particularly those optimised for light-emitting device applications or when measuring samples in solution), this strong fluorescence background can mask the Raman scattering. The extent of this problem depends on the precise wavelength of the excitation and is usually most severe for excitations close to the lowest energy absorption edge, since the absorption and emission spectra overlap most strongly in this region. Alternatively, the photoluminescence itself can be exploited as an additional probe of the sample properties, and it is sometimes possible to separate the Raman and photoluminescence spectra to give simultaneous complementary measurements.[79,80]

A further challenge for resonant Raman spectroscopy of organic semiconductors, is that these materials tend to be photochemically and thermally sensitive. As a result, the photoexcitation and thermal heating of the sample caused by the optical excitation can result in chemical changes and

degradation during the measurement. These effects are reduced by minimising the intensity and duration of optical exposure, or by placing the sample in an inert atmosphere during the measurement to prevent oxidation.

2.2.3. Polarised Raman Spectroscopy

The development and capabilities of polarised Raman spectroscopy for measuring the orientation distributions of molecules has been reviewed comprehensively by Tanaka and Young;[76] below we highlight a few experimental aspects that are particularly relevant to conjugated molecular semiconductors.

Polarised Raman measurements require that both the polarisations of the incident and detected light are controlled. Experimentally, this is typically achieved by using a half-wave plate to rotate the polarisation of the excitation laser beam, and a polariser (often called the analyser) to control the polarisation of the scattered light entering the spectrometer. This approach requires that the excitation source itself is fully linearly polarised, which is a good assumption for laser spectroscopy. However, the polarisation-dependence of the instrument response function must also be considered, and components such as beam-splitters, dichroic filters, and high numerical aperture objectives can alter the polarisation of the light significantly.[81]

Interpretation of polarised Raman spectroscopy data requires a certain amount of information about the sample. In particular, measurements of the molecular orientation require knowledge of the Raman tensors for at least some of the vibrational modes of the molecule. For highly symmetric molecules, the forms of the Raman tensors can be predicted using group theory, but for complex molecules, and particularly polymers, DFT calculations of the Raman tensors are required.[76]

3. Non-Resonant and Polarised Raman Spectroscopy

The frequencies of molecular vibrational normal modes depend on the effective force constants of the vibrating bonds. As a result, they are sensitive to the type of bond and the different atoms involved in the bonding such that the vibrational mode frequencies provide a ‘fingerprint’ for a molecular structure. Infrared absorption spectroscopy can also be used for this sort of chemical analysis as a complementary technique, since the different selection rules of infrared and Raman spectroscopy result in them probing different vibrational modes. As described earlier, the vibrational modes detected by Raman spectroscopy are highly sensitive to the distribution of the π-electron system in conjugated molecules. In particular, the effective conjugation length can be related to the molecular conformation since the strength of the π-bonding depends on the coplanarity of the conjugated part of the molecule. Therefore, the vibrational mode frequencies (and also their Raman cross-sections) provide a spectroscopic probe for the molecular conformation of molecules in a sample. This is a particularly important effect for studies of conjugated molecular semiconductors since the molecular conformation relates closely to the molecular packing and morphology in the solid state, with a significant impact on the resulting device performance. Here we review the use of Raman spectroscopy as a probe for molecular structure, conformation, solid state packing, and orientation by considering a number of published examples.

3.1. Probing Molecular Structure and Conformation

3.1.1. Heteroatom Substitution and Fluorination

One of the simplest chemical changes that can be made to a molecule is the substitution of one atom with another from the same group of the periodic table; often this means replacing a light atom with a heavier one. A substitution of this kind is attractive as a method for tuning the optoelectronic properties of a conjugated semiconductor, and is a common strategy for achieving low energy gap materials. Simplistically, we expect the substitution of one atom with a heavier one to reduce the effective force constant for its bonds giving them lower vibrational frequencies. Experimental results generally support this expectation. Isotopic substitution gives the simplest demonstration, such as the selective deuteration of polythiophene.[82] In this case, deuteration causes a shift in the Raman peak positions towards lower wavenumbers, as expected, but the strongest peaks are much more sensitive to deuteration of the main conjugated backbone than deuteration of the alkyl side chains. A similar effect is observed when the sulfur in polythiophenes is substituted with selenium, where the main Raman peaks of the polyselenophene (P3HS) spectrum are shifted to lower wavenumbers than for polythiophenes (P3HT) – see Figure 6.[83,84] However, this shift is associated not just with the increased mass of the selenium atom, but also with an increase in the delocalisation of the π-electron system due in part to greater coplanarity of the conjugated backbone.[85]

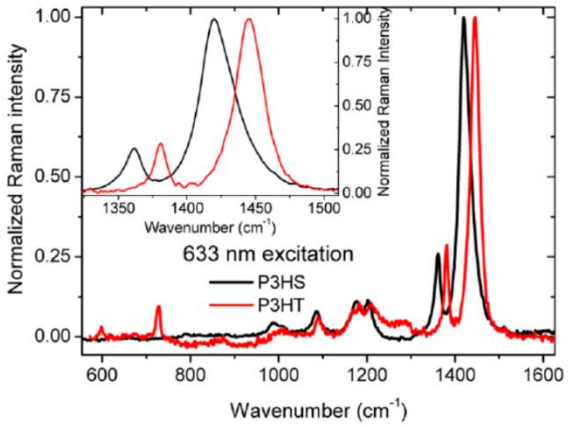

Figure 6. Comparison of Raman spectra for thin films of P3HT and P3HS showing effect of sulfur/selenium substitution. Inset shows detail of main C=C and C-C mode peaks.[84] *Reprinted with permission from W.C. Tsoi et al., ACS Nano, 6, 9646, (2012). Copyright 2012 American Chemical Society.*

Several studies have used Raman spectroscopy to probe the impacts of various atomic substitutions on the properties of conjugated molecules, and have shown that this simple chemical variation has profound effects not just on the force constants of the bonds, but also on the electron density distribution over the molecule, and molecular conformation as well as the molecular packing in the solid state.[84–86]

One class of atomic substitution that has proven particularly useful for enhancing the semiconducting properties of conjugated molecules is fluorination. The replacement of hydrogen atoms with fluorine has a strong electron withdrawing effect from the conjugated part of the molecule, and also modifies the molecular packing. This is exemplified by the case of fluorinated polythiophenes, demonstrated by Figure 7: the two main Raman peaks are commonly referred to as

collective stretches of the C-C and C=C bonds respectively, and both are shifted to higher wavenumbers upon fluorination, indicating increases in the effective force constants for both modes and thus shorter bonds. This is interpreted as in increase in coplanarity of the conjugated backbone of the polymer, but differs from the usual reduction in force constants associated with increased π-electron delocalisation, presumably due to the electron withdrawing effect of the fluorine atoms. The widths of the Raman peaks can also provide structural information. In disordered materials, such as conjugated polymers, vibrational peaks tend to be broad as a result of inhomogeneous broadening where similar bonds in different parts of the molecule have slightly different vibrational frequencies. In this example, the FWHM (full width at half maximum) of the C=C mode peak reduces by a factor of two, indicating a significant reduction in the width of the distribution of different conformations within the solid state sample.[87]

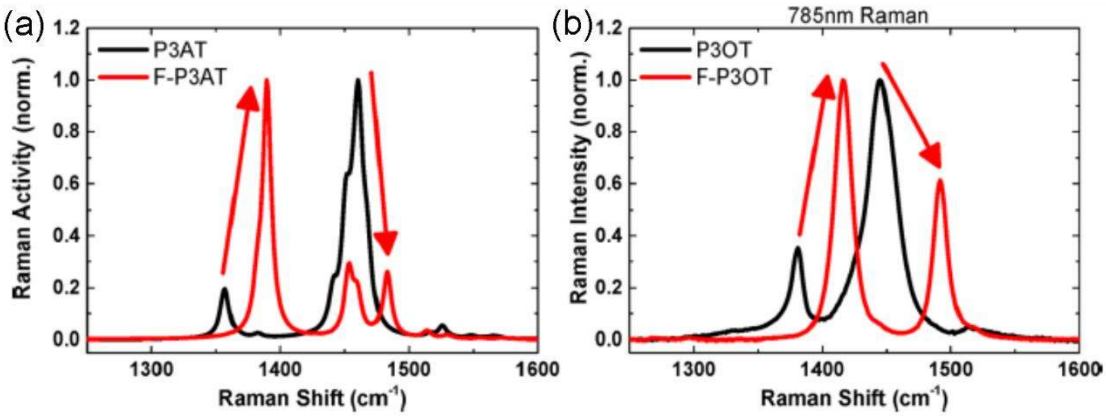

Figure 7. (a) DFT calculated Raman spectra for a polyalkylthiophene (P3AT) a fluorinated polyalkylthiophene (F-P3AT) segment. (b) Experimental Raman spectra for polyoctylthiophene (P3OT) and fluorinated polyoctylthiophene (F-P3OT). Red arrows indicate effects of fluorination on the main Raman peaks. [87] *Reprinted from Z. Fei et al., Journal of the American Chemical Society, 137, 6866, (2015), under CC-BY License. Copyright 2015 American Chemical Society.*

Whilst Raman spectroscopy is clearly a powerful and appropriate probe for the chemical structure and conformation of conjugated molecules, the interpretation of the experimental results becomes increasingly challenging as the structures become more complex. Several groups have successfully applied these methods to donor-acceptor copolymers and considered the effects of various heteroatomic substitutions but the insights gained appear to be rather specific to particular chemical groups and the interpretation relies heavily on corresponding DFT calculations. It is hoped that more general rules and a comprehensive understanding will emerge from ongoing study.[86,88,89]

3.1.2. Side Group Modification

It has already been noted that the optoelectronic properties of conjugated molecules are largely determined by the structure of the conjugated part of the molecule, whereas the side chains are primarily intended as solubilising groups for ease of processing. However, modifications to the side groups can have profound effects on the molecular structure and packing, which are easily detected by Raman spectroscopy. The archetypal example is the comparison of highly regioregular (rrP3HT) and regiorandom poly(hexylthiophene) (rraP3HT) thin films. Both materials have the same conjugated structure so their main Raman peaks are comparable, but display a number of

differences arising from the steric hindrance that makes rraP3HT amorphous, whilst less sterically hindered rrP3HT is semi-crystalline.[90]

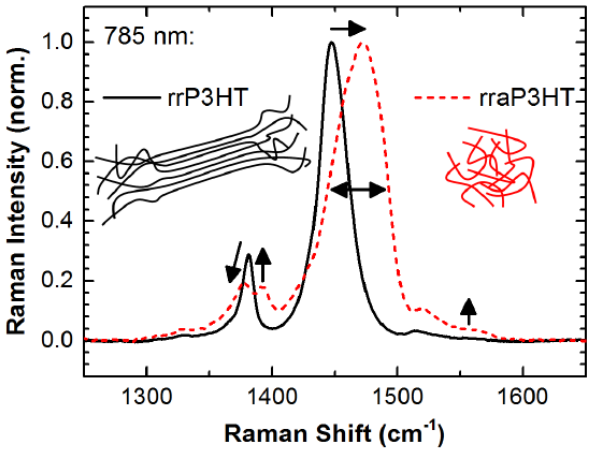

Figure 8. Comparison of main Raman peaks measured for regioregular (rr) and regiorandom (rra) P3HT films using 785 nm, non-resonant excitation. Black arrows indicate main differences and cartoons indicate the molecular packing in each case.

The main differences between the Raman spectra of rrP3HT and rraP3HT, shown in Figure 8, relate to the two strong peaks at around 1380 cm^{-1} and 1450 cm^{-1}. These peaks correspond to collective bond stretching modes of the conjugated polymer backbone and are frequently described as the C-C intra-ring and C=C in-plane symmetric stretching modes, respectively. (In fact, these designations are not readily compatible with the ECCM interpretation outlined above, but are sufficiently entrenched in the literature that they have become useful labels irrespective of their accuracy). In the regioregular case, the majority of inter-unit bonds are head-to-tail resulting in a single C-C peak, whereas the regiorandom material has a large proportion of units subject to a tail-to-tail steric hindrance causing the C-C peak to split into two components (symmetric and asymmetric). The C=C peak is similarly broadened by the wider distribution of conformations in the disordered rraP3HT and the peak position shifts to higher energy. This shift has been associated with the increased localisation of the π-electrons on the thiophene rings arising from strong inter-unit torsion.[90] The intramolecular conformation of P3HT and particularly the coplanarity of the conjugated backbone is strongly correlated with the intermolecular packing and the formation of aggregates such that the measured Raman spectrum can provide a probe for the overall degree of molecular order.[90,91]

Steric effects can also arise through the use of branched or bulky side groups, which manipulate the lowest energy conformation of the molecule and control the dihedral angles at particular positions in the molecular structure.[89,92] In essence, all of these steric effects can be understood in terms of manipulating the effective conjugation length and the impact this has on the Raman spectrum, as discussed in Section 2.1.3.

3.1.3. Hydrostatic Pressure

The examples considered above demonstrate the sensitivity of Raman spectroscopy to changes in the chemical structure of conjugated molecules and the resulting impact on molecular conformation. However, in solid state samples, it is difficult to distinguish the intermolecular (between molecules) and intramolecular (within a molecule) effects associated with molecular

packing. An elegant solution to this problem is found by applying hydrostatic pressure to thin film samples of neat polymer and polymer in a dilute solid state solution.[93] The measured Raman spectrum shows shifts in the peak positions and intensities as a function of applied pressure, which are identified with the enforced planarisation of the molecular structure.[94][95] DFT calculations applying forced dihedral torsions to the inter-unit bonds support the conclusion that the relative intensities of various Raman peaks can be used to experimentally probe the planarity of a conjugated molecular backbone in the absence of any change in the chemical structure.

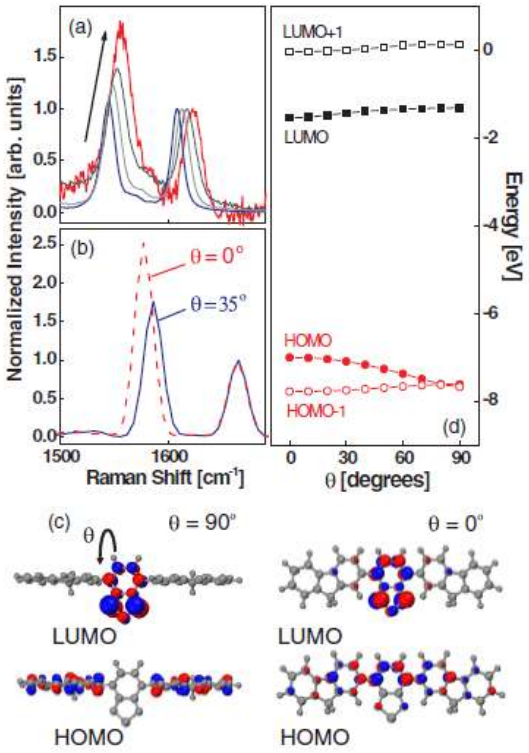

Figure 9. (a) Main Raman peaks of F8BT thin films measured at pressures from 0.1 MPa to 1.8 GPa (arrow indicates increasing pressure), normalised to the intensity of the higher energy mode. (b) DFT calculated Raman activities for an F8-BT-F8 unit with frozen dihedral angle, θ = 0° and θ = 35°. (c) DFT calculated HOMO and LUMO topologies with θ = 90° and θ = 0°. (d) DFT calculated energies of the HOMO - 1, HOMO, LUMO, and LUMO + 1 as a function of θ.[93] *Reprinted figure with permission from J.P. Schmidtke et al., Physical Review Letters, 99, 167401, (2007). Copyright 2007 by the American Physical Society.*

Pressure-dependent Raman spectra of the alternating copolymer of fluorene with benzothiadiazole (F8BT) is shown in Figure 9 alongside corresponding DFT calculations. This work established a link between the inter-unit dihedral torsion angle and the relative intensities of the ring stretching modes associated with the fluorene (1545 cm^{-1}) and benzothiadiazole (1608 cm^{-1}) units respectively.[93,96] We note an apparent disagreement between this work and a more recent study considering the position of the benzothiadiazole unit within a quaterfluorene chain, which attributes a similar experimental observation to variation in the natural transition orbital probability density distribution without change in the torsion angle.[97] These two concepts are readily reconciled by recognising that both molecular conformation and chemical structural differences can affect the molecular orbital distributions (as shown in Figure 9(c)), which affect the Raman scattering cross-sections.

In addition to using pressure-dependent Raman spectroscopy to probe changes in the conformation of conjugated molecules, a lack of change during these experiments can also provide useful information: the measured independence of the relative intensities of Raman peaks as a function of applied pressure indicates that the molecule is already highly planar with a narrow distribution of conformational states.[98]

3.1.4. Processing Conditions

The morphology of conjugated molecular thin films is also strongly dependent on the conditions under which the material is deposited, and many published studies have applied Raman spectroscopy as a probe of this morphology. Here we select a few of the many examples, which offer the most instructive insights.

In general, the Raman spectra of small conjugated molecules are simplest to understand because symmetry considerations allow clear identifications of the observed modes, and many small molecules display distinct, and well-known, polymorphs. The acenes, particularly pentacene, have attracted a great deal of attention and show clear differences in the Raman spectra of films deposited under different conditions.[99,100] Figure 10 compares experimental spectra for pentacene films grown on various different surfaces, with the overlapping contributions fitted with Gaussian/Lorentzian peak shapes. Clear differences are observed in the band from 1150 cm^{-1} to 1170 cm^{-1} corresponding with C-H bending modes, including both variation in the relative intensities of the three contributions, and a splitting between the 1155 cm^{-1} and 1158 cm^{-1} peaks. These effects are attributed to Davydov splitting (also called factor-group splitting) where bands in the vibrational or electronic spectrum of a crystal are split in energy due to the unit cell containing more than one equivalent entity.[101] In this case the two molecules in the unit cell of the pentacene crystal experience different intermolecular interactions such that the C-H bending mode has different frequencies for the two cases. A key feature of Davydov splitting is that the two modes have different polarisation properties, which is observed in this case.[100] Since this effect arises only when the molecules are in a crystalline morphology, the Raman spectrum can be used as a probe for this morphology.

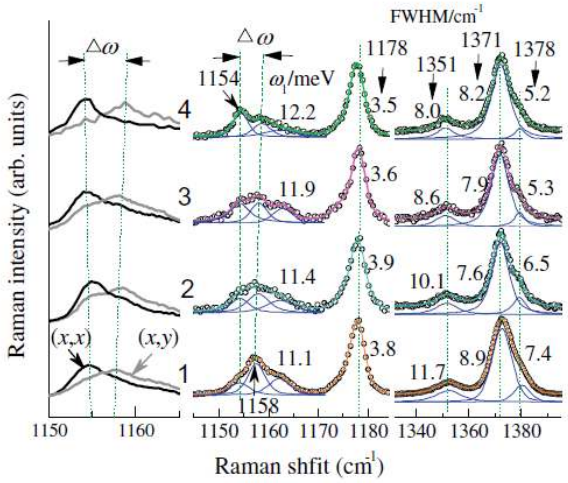

Figure 10. (Right) Comparison of main Raman peaks of pentacene films grown on (1) thermally grown SiO_2, (2) chemical vapour deposited SiO_2, (3) polymethylmethacrylate, and (4) polyimide surfaces, measured with 532 nm excitation. Gaussian/Lorentzian peak fitting contributions shown.

(Left) Polarised components of Raman peak measured with 633 nm excitation with the poalrisations of incident and detected light: parallel (x,x) and perpendicular (x,y).[100] *Reprinted from H.-L. Cheng et al., Organic Electronics, 10, 289, (2009), Copyright 2009, with permission from Elsevier.*

A recent study considering the use of different deposition conditions for 9,10-diphenylanthracene crystals was able to identify three polymorphs by their distinctive Raman spectra.[102] In this case, the clearest differences lie in the low wavenumber region (< 200 cm^{-1}), corresponding to vibrations of the crystal lattice, and are compared in Figure 11. This region of the Raman spectrum is particularly useful for identifying polymorphs of crystalline molecules and even assessing the phase purity.[103,104]

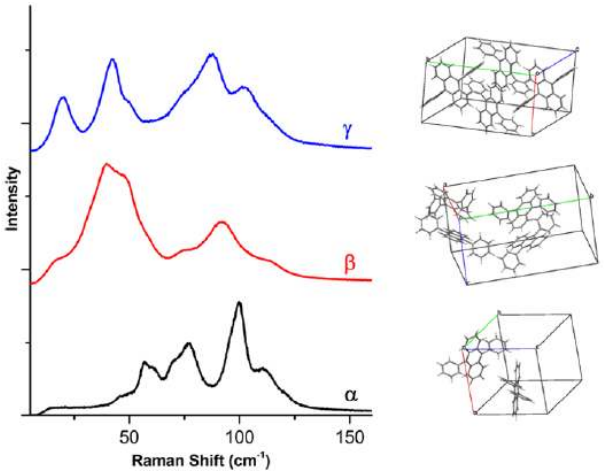

Figure 11. Comparison of low wavenumber experimental Raman spectra for the three polymorphs of 9,10-diphenylanthracene identified (α,β,γ) alongside their corresponding unit cells.[102] *Reprinted with permission from T. Salzillo et al., Journal of Physical Chemistry C, 120, 1831, (2016). Copyright 2016 American Chemical Society.*

Some conjugated polymers can be described as semi-crystalline, and display a number of different phases in the solid state, depending on the processing conditions such as the choice of solvent used for the deposition or thermal annealing. Among the first such materials to be considered in this way using Raman spectroscopy is polyfluorene, whose Raman spectrum shows a sensitivity to such processing conditions, as illustrated by Figure 12 (note that there is a spectroscopic tradition of displaying Stokes-shifted Raman spectra with wavenumbers increasing from right to left, though this is not strictly observed).

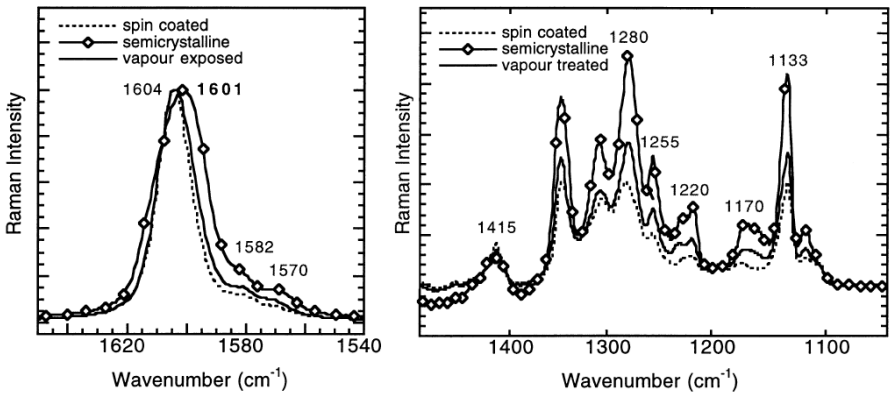

Figure 12. Comparison of Raman spectra of poly(9,9'-dioctylfluorene) (F8) measured using 633 nm excitation for: spin-coated (glassy), semi-crystalline (thermally annealed), and vapour treated (extended intrachain conformation) samples.[105] *Reprinted from M. Ariu et al., Synthetic Metals 116, 217, (2001). Copyright 2001, with permission from Elsevier.*

Many of the observed variations are subtle changes in the shapes, positions and intensities of many different peaks in the Raman spectrum, which are not trivial to interpret. Attention is generally focused on the symmetric stretching modes associated with the conjugated backbone since these are experimentally easy to measure and can be broadly understood in terms of π-electron delocalisation and backbone planarity. However, detailed studies making use of combined DFT and experimental results for oligomers of different lengths have been able to interpret many of the spectral changes associated with different phases of polyfluorene.[106,107] One example is that the enhanced backbone planarity of β-phase of dioctyl substituted polyfluorene arises from a specific conformation of the alkyl side chains.[108] An analogous study of oligothiophenes and poly(hexylthiophene) has also been performed, identifying multiple structural markers across the whole range of molecular vibrational modes revealing both the backbone and side chain conformations.[109]

3.1.5. Chemical Composition Mapping

The chemical sensitivity of Raman spectroscopy makes it an appropriate technique for spatially resolved measurements of the composition of microstructured samples, with diffraction-limited resolution. [110] Figure 13 shows a chemical map of polyfluorene nanowires formed on a silicon/polytetrafluoroethylene (PTFE) substrate, obtained by plotting the integrated intensity of the characteristic polyfluorene 1605 cm^{-1} Raman scattering peak.[111]

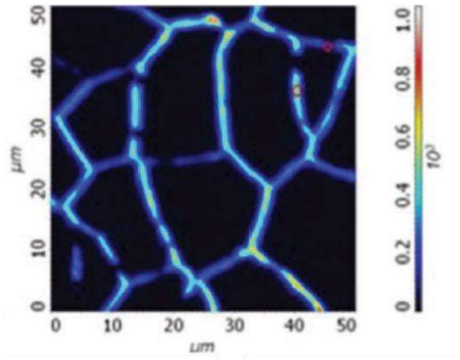

Figure 13. Mapping of the integrated intensity of the 1605 cm^{-1} Raman mode of polyfluorene deposited on a PTFE surface showing nanowires formed by dewetting.[111] *Reprinted with permission from S.S. Chang et al., Advanced Functional Materials, 20, 18, (2010), Copyright 2010 WILEY-VCH Verlag GmbH & Co. KGaA, Weinheim.*

Raman mapping offers some distinct advantages over photoluminescence imaging, which can also be used for chemical mapping. Firstly, Raman spectroscopy enables a greater degree of specificity, since many conjugated molecules have overlapping photoluminescence spectra, whereas distinctive Raman peaks can usually be found. Secondly, Raman mapping can give a more quantitative measure of the composition of the sample, in addition to detailed morphological information (see Section 3.1.4). This kind of quantitative analysis has been demonstrated for a blend of two conjugated polymers, known as F8BT and TFB, where the Raman spectra at two different positions are compared to reference spectra for neat materials to measure the purities of the phase-separated domains in blend thin films (see Figure 14). [112]

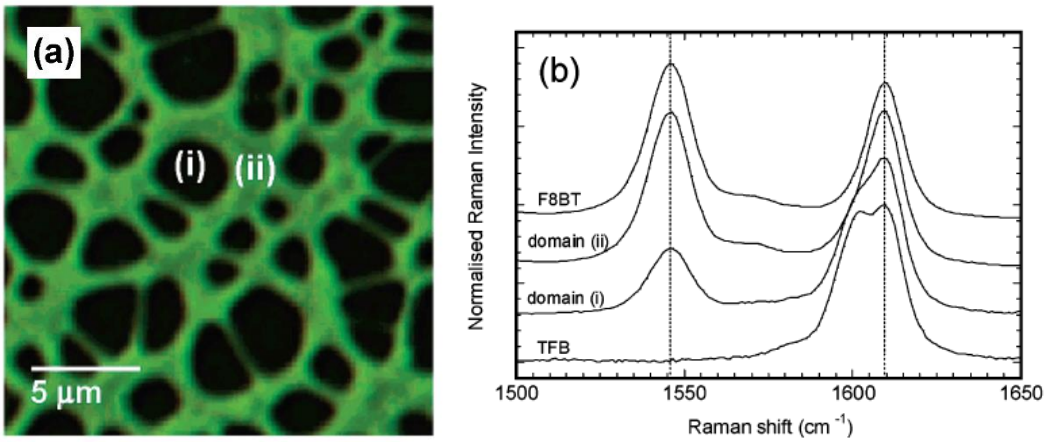

Figure 14. (a) Photoluminescence intensity map of F8BT:TFB blend film. Regions (i) and (ii) are identified as TFB-rich and F8BT-rich, respectively by comparing their Raman spectra with those of neat TFB and F8BT films, shown in (b).[112] *Reprinted with permission from J.-S. Kim et al., Macromolecules, 37, 2861, (2004). Copyright 2004 American Chemical Society.*

3.2. Probing Molecular Orientation

The polarisation dependence of Raman scattering provides a means by which Raman spectroscopy can probe the orientation of conjugated molecules. For polymeric materials, thin film samples have limited anisotropy, but it is possible to identify a tendency for the molecules to adopt a particular orientation.[113][114] However, in more highly ordered samples, such as molecular crystals,

polarised Raman measurements can be used to provide a more quantitative measure of molecular orientation.

Pentacene, and its soluble derivatives, are a good model system for polarised Raman measurements, since it has two strongly Raman active vibrational modes with distinct Raman tensors: an A_g mode around 1371 cm^{-1} and a B_{3g} mode around 1596 cm^{-1}, which have the following forms for a molecule in the Cartesian coordinate orientation indicated in Figure 15:

$$\boldsymbol{R}(\boldsymbol{A_g}) = \begin{pmatrix} a & 0 & 0 \\ 0 & b & 0 \\ 0 & 0 & c \end{pmatrix} \qquad \boldsymbol{R}(\boldsymbol{B_{3g}}) = \begin{pmatrix} 0 & 0 & 0 \\ 0 & 0 & d \\ 0 & d & 0 \end{pmatrix} \tag{12}$$

The intensities of these two modes therefore provide a probe for the orientation of the molecule.[115] Several groups have applied this technique to study how different deposition conditions determine the orientation of the semiconducting molecules.[115–118] The Raman scattering intensities of particular modes are often plotted against the angle of the incident light polarisation (for a fixed analyser position) on polar axes, which produces a 'peanut' shaped plot if the sample is anisotropic, or a circle for an isotropic sample. Figure 15 illustrates this for an ink-jet printed spot of the soluble pentacene derivative 6,13-bis(triisopropylsilylethynyl)-pentacene (TIPS-pentacene). This is a good way of visualising the degree of anisotropy or variation in molecular orientation, but some caution is required since the relationship between the orientation of the 'peanut' and the locus of possible orientations of the molecule is not obvious as a result of the tensorial nature of the governing equation (Equation 11).

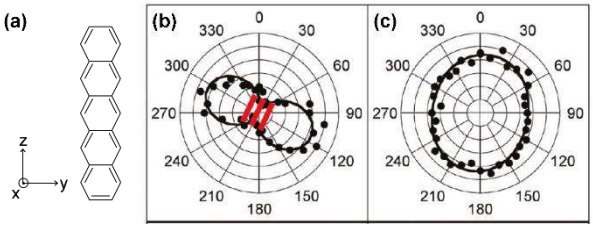

Figure 15. (a) Molecular structure of pentacene with Cartesian coordinate system. (b) and (c): Polar plots showing Raman intensity of the 1374 cm^{-1} mode of TIPS-pentacene plotted over incident polarisation angles from 0° to 360°, comparing inkjet printed spots deposited on two different surfaces resulting in anisotropy values of 0.84 and 0.33, respectively. Proposed TIPS-pentacene backbone orientation shown as red bars.[117] *Reprinted with permission from D.T. James et al., ACS Nano 5, 9824, (2011). Copyright 2011 American Chemical Society.*

A similar example explores how the tilt angle of the acene core relative to the plane of the substrate can be controlled by first treating the gold surface with a self-assembled monolayer before vacuum deposition of the pentacene. By varying the thickness of the pentacene film it was also possible to probe the difference in molecular orientation at the interface and in the bulk of the film. [17] The technique can be readily extended to give spatially resolved mapping of variations in molecular orientation.[17,115–117] In principle, polarised Raman measurements are able to give a precise measurement of molecular orientation, which has recently been demonstrated for a single-crystal organic transistor.[119]

4. Resonant Raman Spectroscopy

Since most organic semiconductors have strong optical absorption transitions in the visible range, resonantly enhanced Raman scattering can often be achieved by choosing an appropriate excitation wavelength with reference to the absorption and emission spectra of the material or materials in a sample. The intensity enhancement afforded by resonance makes it particularly easy to obtain strong signals in many cases, as well as providing a probe for additional information that is not available from non-resonant Raman spectroscopy, as we consider below.

4.1. Chemically Selective Excitation

Typical organic semiconductor devices are composed of multiple different materials either blended together or combined in layers, several of which might display strong Raman scattering or photoluminescence. As a result, it can be difficult to measure the Raman scattering from one particular component if the contributions from other components are dominant. For example, in a hybrid organic-inorganic blend system of CdS nanoparticles and P3HT, the Raman scattering from the CdS is much weaker than the scattering from the P3HT under non-resonant conditions and so the main CdS Raman peak (303 cm^{-1}) in a blend film cannot be resolved clearly. This problem can be overcome by considering the absorption spectra of the two materials separately, as shown in Figure 16, and selecting an excitation wavelength that will result in comparable Raman scattering intensities by exploiting the resonant enhancement.[120,121] In this case, the CdS has a larger energy gap than P3HT so a short wavelength excitation is required to give a suitable resonant enhancement. In this case, 457 nm falls within the absorption band of CdS and in the tail of the optical absorption band for P3HT so both materials display resonantly enhanced Raman scattering. It is, therefore, possible to observe the main Raman peaks from both materials simultaneously, as shown below.[122]

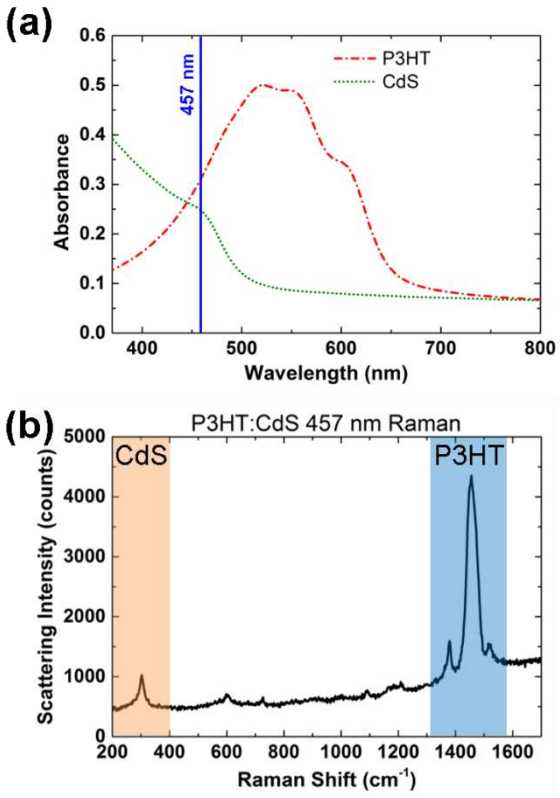

Figure 16. (a) Thin film absorbance spectra of P3HT and CdS with blue line indicating spectral position of 457 nm Raman excitation laser. (b) Resonant Raman spectra of P3HT:CdS blend film measured using 457 nm excitation. Orange and blue shaded regions indicate main Raman modes originating from the CdS and P3HT, respectively.[122] *Adapted from S. Wood et al., Faraday Discussions, 174, 267, (2014) by permission of The Royal Society of Chemistry.*

In practice, the selection of appropriate measurement conditions for a particular sample requires some optimisation and a trial-and-error approach. To some extent, an educated choice can be made by considering the absorption and emission spectra of the component materials to identify suitable resonant enhancements and problematic photoluminescence features, but the relative magnitudes of these effects cannot be estimated by simple methods. Fortuitously for blended organic semiconductors, the photoluminescence, which can present a problem for resonant Raman spectroscopy measurements, is often strongly quenched by charge transfer between the two species and so poses a reduced challenge.[91,121]

It is important to note that the resonant enhancement does not preserve the shape of the Raman spectrum since the different modes experience different enhancements, as discussed in Section 2.1. Typically, the resonant Raman spectrum has fewer modes than the non-resonant case because the electronic-vibrational coupling is strongest for the vibrational modes associated with the conjugated part of the molecule such that the resonantly enhanced modes are those containing strong components of the $\mathcal{A}$ mode coupled to the electronic transition.

4.2. Morphological Characterisation of Polymers

The sensitivity of the Raman spectra of conjugated molecules to morphological variation was described in Section 3.1.4 for measurements under non-resonant conditions. The extension into the resonant regime provides an additional level of sensitivity, as well as experimental advantages

associated with an enhanced signal. For conjugated molecules, the main resonantly enhanced modes correspond with collective vibrational stretching modes of the conjugated backbone, which display a particular sensitivity to the conformation of this part of the molecule and are closely related to the semiconducting properties of the material.

4.2.1. Morphologically Selective Excitation

For the archetypal organic photovoltaic device comprising a blend of P3HT with the fullerene derivative phenyl-C_{61}-butyric acid methyl ester (PCBM), thermal annealing is known to be an effective strategy for controlling the morphology of the active layer to enhance the device performance. We have already seen that non-resonant Raman spectroscopy is sensitive to this type of morphological change,[123] but Figure 17 compares the sensitivity of the non-resonant (or quasi-resonant) Raman spectrum measured using 633 nm excitation, with that measured under fully resonant conditions using 488 nm excitation.[90] In both cases there are visible differences in the main Raman peaks for the P3HT in the blend film with and without thermal annealing, but the variation is much clearer in the resonant case. This can be understood in terms of the optical absorption spectra of the ordered and disordered polymer phases present in the sample: the disordered P3HT absorption band has its peak at shorter wavelengths than that of the ordered phase (around 440 nm vs 520 nm) and so the 488 nm excitation has a stronger resonance with the disordered component.[90] In effect, this resonant enhancement provides a selective probe with particular sensitivity to the disordered polymer phase.[124]

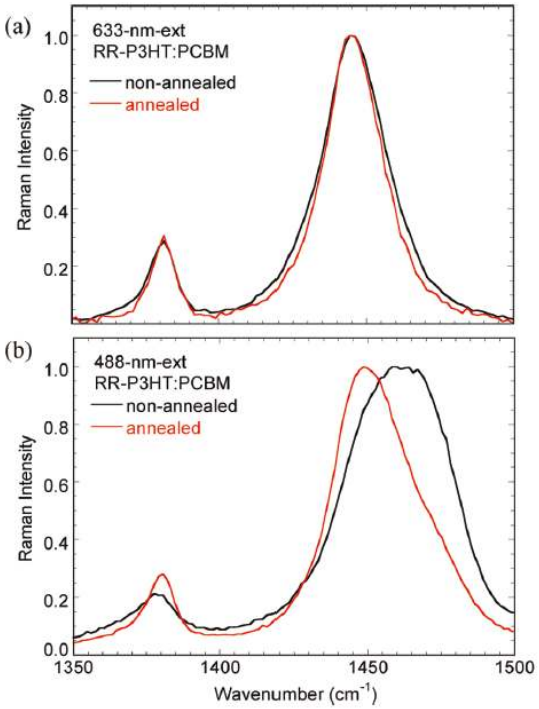

Figure 17. Comparison of main Raman peaks in experimental spectra for thin films of annealed and non-annealed regioregular P3HT:PCBM blends, measured using (a) 633 nm, and (b) 488 nm excitation.[90] *Reprinted with permission from W.C. Tsoi et al., Journal of the American Chemical Society, 133, 9834, (2011). Copyright 2011 American Chemical Society.*

In reality, conjugated polymer films contain a continuous distribution of molecular conformations and cannot simply be described as a linear combination of two phases (ordered and disordered),

however, the two-phase model does permit a semi-quantitative analysis of a sample. This was first demonstrated by fitting the broad main peak (1450 cm^{-1} to 1470 cm^{-1}) with two Lorentzian peak shapes representing the two phases, and subsequently, using experimental reference spectra taken from neat films of regioregular and regiorandom P3HT (see Figure 18).[90,91] The advantage of the latter method is that the proportions of the two contributions can be quantitatively related to actual percentages of the two phases present in the sample. However, care must be taken to account for the different Raman scattering cross-sections of this vibrational mode for the two different conformational phases, and it is important to recognise that the reference samples themselves are not pure ordered and disordered phases. Therefore the calculated degree of molecular order is a relative value, providing a quantitative measure with respect to the extremes set by the neat rraP3HT and neat rrP3HT reference samples.[80]

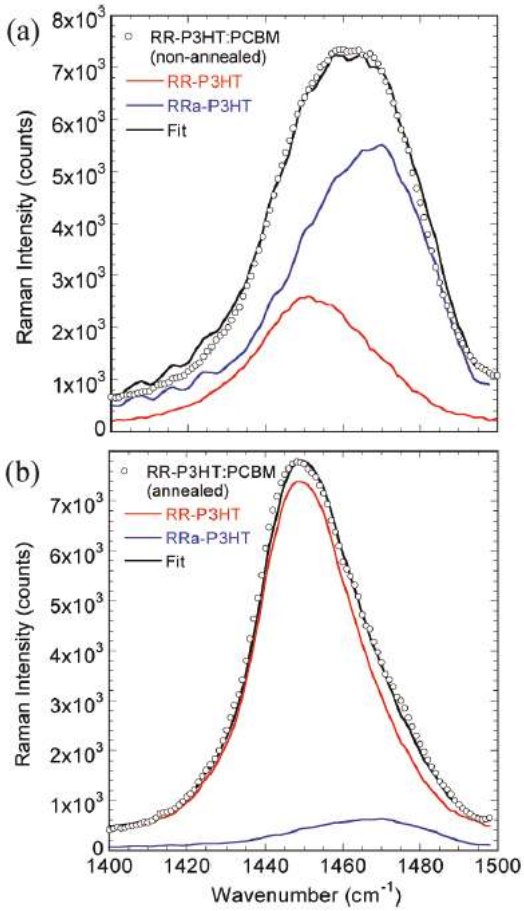

Figure 18. Fitting the main Raman peak measured using 488 nm excitation for (a) non-annealed and (b) annealed regioregular P3HT:PCBM blend films using a linear combination of peaks measured for regioregular P3HT (RR-P3HT) and regiorandom P3HT (RRa-P3HT) reference samples.[90] *Reprinted with permission from W.C. Tsoi et al., Journal of the American Chemical Society, 133, 9834, (2011). Copyright 2011 American Chemical Society.*

It is increasingly recognised that morphological models of organic semiconductors need to accommodate more than two phases. An example of this is the distinct 'nanowire' morphology of P3HT, where careful control of solution conditions can make the polymer chains aggregate into long, thin structures roughly 20 nm across and 1 µm long. This morphology represents a highly ordered packing structure, and a further distinction has also been made between H- and J-type aggregation

within the nanowires, where the different packing motifs in each case have a strong effect on the optoelectronic properties of the material.[125,126]

A striking feature of resonant Raman spectra for conjugated polymers is that they frequently show strong series of overtone and combination progressions as illustrated in Figure 19 for P3HT:PCBM blend films. The interpretation of these overtones has recently been discussed by Grey and co-workers in terms of the time-dependent theory of Raman spectroscopy, producing some degree of qualitative agreement between experimental and simulated results, though there remain substantial discrepancies attributable, at least in part, to experimental limitations.[127–129] By fitting the model to the absorption and Raman spectra a series of vibrational coordinate displacement values, Δ_k, can be obtained for the vibrational modes, k, where Δ is the dimensionless displacement of the electronically excited state potential energy surface with respect to the ground state potential energy surface along the vibrational coordinate of that mode (see ΔQ_j, in Section 2.1.2). The time-dependent model used to calculate the overtone intensities also provides an interpretation in terms of ultrafast (<100 fs) dynamics.[128][130] Significantly, this means that resonance Raman spectroscopy can be used to probe the conformational geometry of the excited state and dynamics, albeit in a limited way, without the need for complex time-resolved measurements.

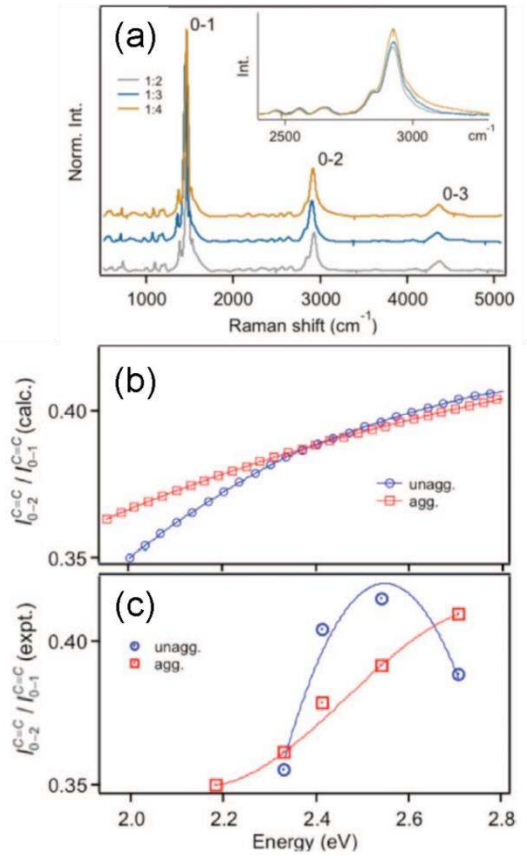

Figure 19. (a) Resonant Raman spectra of P3HT:PCBM blend films with weight ratios 1:2, 1:3, and 1:4. Inset: detail of 0-2 overtone peak. (b) Calculated, and (c) Experimental ratios of overtone to fundamental intensity ratios for main P3HT C=C peak plotted against excitation energy for aggregated and unaggregated polymer. Trends highlighted using polynomial fitting lines.[128] *Reprinted from J. Gao and J.K. Grey, Journal of Chemical Physics, 139, 044903, (2013), with the permission of AIP Publishing.*

4.2.2. Morphological Mapping

Having established the sensitivity of resonant Raman spectroscopy to morphological variation within an organic semiconductor sample, the conversion of this measurement into a spatial mapping technique is a relatively simple extension, made practical by the strong resonant signal enhancement, which allows high resolution imaging in short periods of time.[91,129]

The example shown in Figure 20 considers the morphological impact of excessive thermal annealing on a P3HT:PCBM blend film, where the main P3HT Raman peak measured at each pixel has been fitted with two Lorentzian contributions representing the aggregated and unaggregated polymer phases. The maps show the spatial distribution of the overall Raman intensity and the ratio of aggregated to unaggregated P3HT, given by $R = I^{agg.}_{C=C} / I^{un.}_{C=C}$. The 'over-annealed' blend film shows a ~5 µm feature with low overall P3HT content and a high proportion of unaggregated polymer, which is identified as a PCBM crystallite.[91]

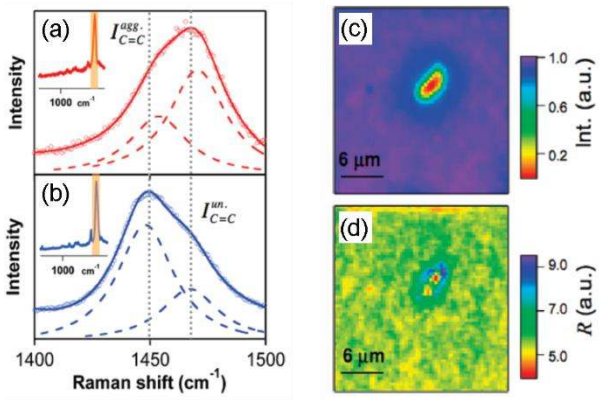

Figure 20. Raman spectra of (a) as-cast, and (b) annealed P3HT:PCBM blend films showing the main P3HT C=C peak fitted with two Lorentzian functions corresponding with aggregated and unaggregated components. (c) Normalised intensity map, and (d) map of R values for an 'over-annealed' P3HT:PCBM blend film showing a PCBM crystallite in the centre.[91] *Reprinted with permission from Y. Gao and J.K. Grey, Journal of the American Chemical Society, 131, 9654, (2009). Copyright 2009 American Chemical Society.*

4.3. Nature of Optical Absorption Transitions

Much of the current understanding of Raman spectroscopy of conjugated molecules is based on studies of relatively simple cases, where the relevant vibrational modes couple to a single electronic transition, as crystallised in the ECCM (see Section 2.1.3). However, many of the materials which have now been developed for organic semiconductor applications do not appear to fit this paradigm, in particular the donor-acceptor class of copolymers and small molecules.

4.3.1. Donor-Acceptor Copolymers

Donor-acceptor molecules are expected to have an optically active electronic transition representing charge transfer from one moiety (electron donor) to another (electron acceptor) resulting in a 'charge transfer' band in the absorption spectrum, typically in the visible range. The clearest example of this is F8BT, which has an obvious 'camel-back' absorption spectrum with peaks at around 320 and 460 nm. Computational studies have assigned the higher energy transition to the formation of a delocalised excited state (π-π* transition) and the lower energy transition to a charge transfer transition to an excited state localised on the benzothiadiazole acceptor unit.[131,132]

Resonant Raman spectroscopy provides an experimental technique to complement these theoretical results by probing the natures of the various optical absorption transitions observed in conjugated molecules.

Many different donor-acceptor copolymer structures have been designed and synthesised incorporating a large number of different electron donating or accepting units. Among these, the benzothiadiazole acceptor unit is particularly common, and its copolymers typically have comparable optoelectronic properties to F8BT. Resonant Raman spectroscopy studies on several members of this copolymer family have been undertaken, where a range of different excitation wavelengths are used to explore the various resonances across the absorption bands.[86,133] The relative strengths of the resonant enhancements for the various Raman peaks at different excitation wavelengths indicate which parts of the molecule are geometrically distorted in the excited state corresponding with the resonant optical transition. In effect, the strongest Raman peaks for the different excitation wavelengths provide a map of which parts of the electronic wavefunction are most affected by the transition. Figure 21 summarises these results for PCDTBT (polycarbazole donor with benzothiadiazole acceptor and bridging thiophene units), where the 457 nm excitation falls within the lower energy absorption band and 1064 nm is a non-resonant excitation. The study also used 351 nm excitation to probe the higher energy transition. Attention is drawn to the enhancement of the peak at 1374 cm^{-1} under 457 nm excitation, which is assigned to a vibrational mode localised on the acceptor unit. This result is interpreted to show that the corresponding electronic transition has the character of charge transfer from the donor to the acceptor unit, in agreement with DFT calculations.[86]

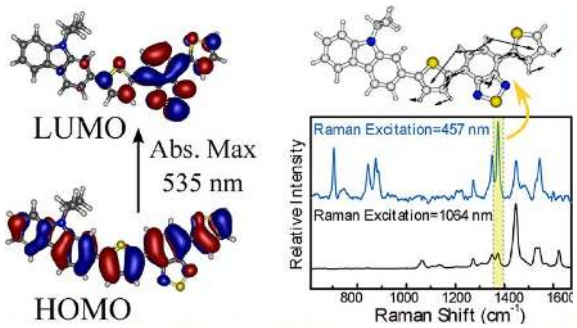

Figure 21. (Left) Electron isodensity surfaces from DFT simulations, showing HOMO and LUMO of PCDTBT. (Right) Raman spectra of PCDTBT measured using 457 nm excitation to resonantly probe the lowest energy absorption band, and non-resonant excitation at 1064 nm. Highlighted mode corresponds with the illustrated vibrational mode localised on the benzothiadiazole unit.[86] *Reprinted with permission from M.E. Reish et al., Journal of Physical Chemistry C, 116, 21255, (2012). Copyright 2012 American Chemical Society.*

This experimental confirmation of the established theory appears to hold for all of the benzothiadiazole-based copolymers which have been studied, but there is some debate over how generally these findings can be applied across the whole range of donor-acceptor molecules.[134–136] The next section considers one such case.

4.3.2. Diketopyrrolopyrrole (DPP)-Based Copolymers

The diketopyrrolopyrrole (DPP) unit has found widespread use in low energy gap copolymers and small molecules for various types of organic semiconducting device, yielding good device performances on account of their highly planar conjugated backbones and ambipolar charge

transport.[137][16] DPP is usually considered to be an electron accepting unit, so is copolymerised with an electron rich unit, in this example, triselenophene. The thin film absorption spectrum of this material (known as DPPB-3Se) is shown in Figure 22 and has two absorption bands within the visible range. However, in contrast to copolymers based on the benzothiadiazole unit, the higher energy band is significantly weaker than the low energy band. This indicates a difference between these two families of copolymers, which becomes clear when resonant Raman spectroscopy is used to investigate the natures of these two absorption transitions in detail.

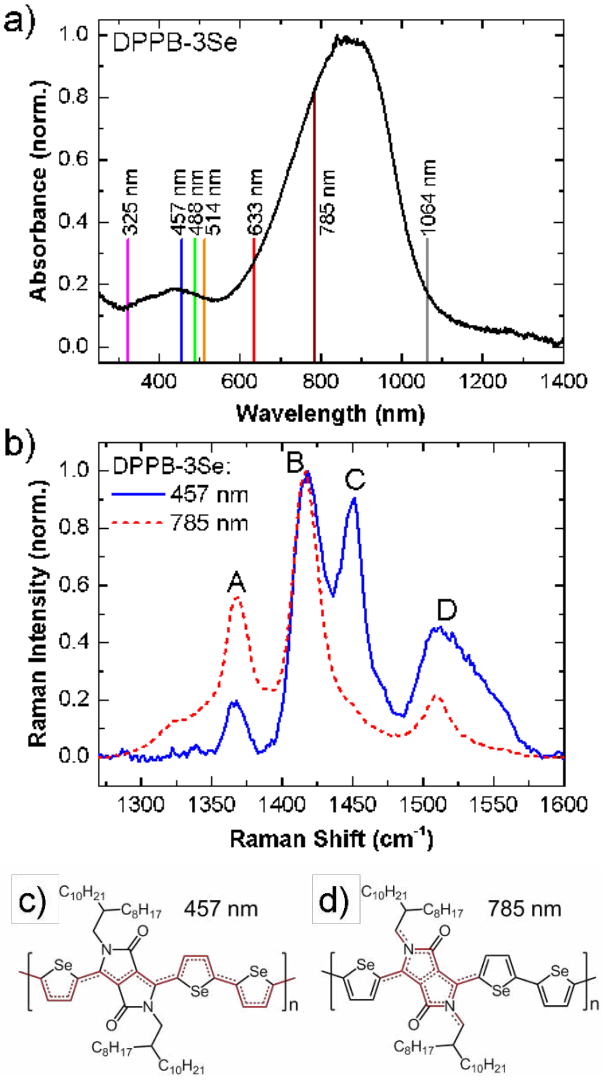

Figure 22. (a) Normalised thin film absorption spectrum of DPPB-3Se showing spectral positions of the Raman excitation lasers used in the study. (b) Comparison of normalised resonant Raman spectra of DPPB3-Se measured using 457 nm and 785 nm excitations with main modes A, B, C, and D labelled. (c) and (d) show the chemical structure of DPPB-3Se with red regions indicating which parts of the molecule experience the greatest geometric distortion during optical excitation at 457 nm and 785 nm, respectively.[54] *Adapted from S. Wood et al., Energy and Environmental Science, 8, 3222, (2015) by permission of The Royal Society of Chemistry.*

The nature of these two absorption bands was probed by measuring resonant Raman spectra using excitation wavelengths aligned with the two absorption peaks: 457 and 785 nm. In this example, the important observation is that the 1450 cm^{-1} peak (mode C in Figure 22(b)), assigned to the C=C

symmetric stretching mode on the selenophene ring is clearly enhanced under 457 nm excitation, but almost completely absent under 785 nm excitation. This reveals that the π-electron density on the selenophene unit is redistributed by the high energy optical transition, but not affected by the low energy transition. Figure 22(c) and (d) illustrate the conclusion regarding which parts of the molecule are involved in optical transitions for each of the main absorption bands. This conclusion is difficult to reconcile with the traditional donor-acceptor paradigm of F8BT, where the low energy transition is understood to transfer π-electron density from the donor unit to the acceptor.[54] We note that the experimental observations regarding the resonant enhancements of Raman modes associated with the donor and acceptor units are actually quite similar in the DPP case to the studies of benzothiadiazole-based polymers discussed above, though the interpretations of these observations are somewhat divergent – it is hoped that future investigations will clarify how these data should be understood correctly.

5. *In Situ* Characterisation

The non-invasive and non-destructive nature of Raman spectroscopy lends itself well to the characterisation of samples and devices as they evolve under operational or controlled conditions. Such *in situ* measurements are typically achieved using a sample chamber that allows the conditions experienced by the sample (*e.g.* temperature, pressure, atmospheric composition, light exposure, or electrical bias) to be controlled, whilst maintaining optical access for the spectrometer. By measuring samples *in situ* it is possible to obtain much more information about the behaviour of conjugated materials and any critical transitions that might occur during their use in operational devices. Here we will discuss some specific applications of *in situ* characterisation that involve conditions relevant to conjugated polymers and organic electronic devices.

5.1. Thermal Stability and Phase Transitions

5.1.1. Temperature-Dependent Raman Spectroscopy

The material, optoelectronic, and chemical properties of conjugated molecular semiconductors all have important dependencies upon temperature. These are relevant for both device manufacture, where temperature control and thermal treatment are often required in the processing, and for device operation, which requires stable performance over a range of thermal conditions. For these reasons, *in situ* studies of organic electronic samples under temperature-controlled conditions are particularly valuable and Raman spectroscopy is found to be an especially appropriate probe (see examples below). However, care is required in the interpretation of the data because the Raman spectra measured for a conjugated molecule at different temperatures depend on multiple effects. Some of these effects are illustrated in Figure 23, which considers changes in the Raman spectrum of polyfluorene with temperature. In this case, the spectral position of the main fluorene ring-stretching mode at around 1605 cm^{-1} and the FWHM of this peak show both a monotonic trend from 50 °C to 350 °C on both heating and cooling, as well as a series of sharper features centred on particular temperatures. The monotonic trend is assigned to the effects of anharmonic interactions, where the vibrational modes broaden and shift towards lower energies at elevated temperatures (*i.e.* the energy level spacing for a vibrational mode progression reduces for higher states, which are more populated at increased temperatures).[138] This effect is expected to be reversible upon cooling, but the measured data show a clear non-reversibility, which indicates that permanent changes in the sample arise from this treatment. The sharper features in the plots (labelled A-F) are assigned to phase transitions, and it is found that the measured depolarisation ratio (defined in

Section 2.1.4) of the Raman scattering is a good probe for these effects. These measurements are typically performed with the sample in an inert atmosphere to prevent chemical degradation, since conjugated molecules show increased susceptibility to oxidation at elevated temperatures. In principle, we would expect the heating and cooling traces in these plots to match up at the highest temperature recorded, but these data show offsets implying a delay or some change in measurement conditions between the heating and cooling measurements.[113]

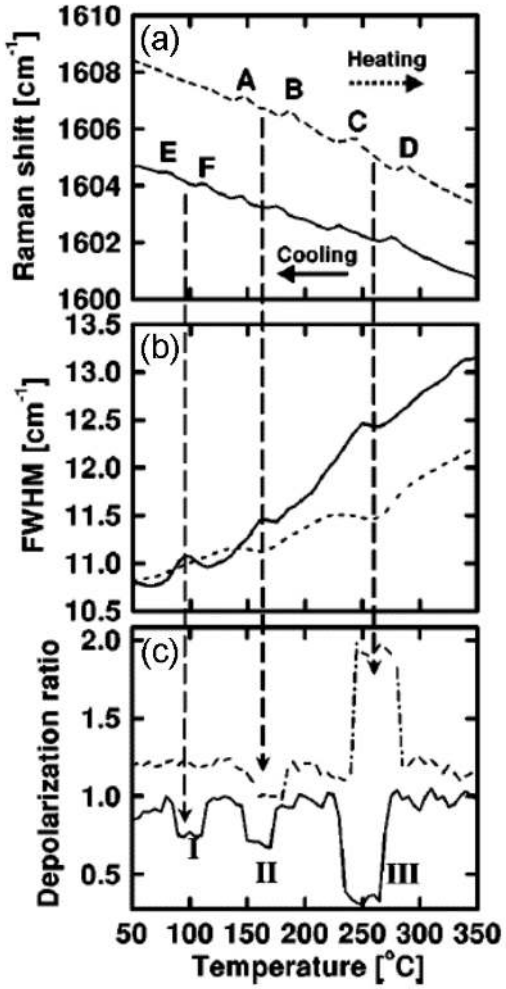

Figure 23. Temperature-dependent Raman scattering parameters measured for a poly(9,9-dihexylfluorene) thin (100 nm – 150 nm) film plotted for heating then cooling between 50 °C and 350 °C: (a) peak position, (b) FWHM, and (c) depolarisation ratio of main fluorene ring stretching mode.[113] *Reprinted from H. Liem et al., Journal of Applied Physics, 92, 1154, (2002), with the permission of AIP Publishing.*

5.1.2. Thermal Annealing and Thermal Stability

Morphological changes in an organic blend film are particularly relevant for photovoltaic applications, where devices are expected to operate at elevated temperatures (up to 80 °C) and long-term stability in device performance is required.[45] Frequently, the optimum morphology for device performance is far from thermodynamic equilibrium, and thermally activated changes in that structure will compromise efficiency.[139]

The morphological evolution of organic blend film devices can be explored by applying the morphological characterisation techniques described in Section 4.2 to Raman spectra measured under thermally controlled conditions. This is exemplified using a P3HT:PCBM blend; Figure 24 shows the peak position of the main C=C stretching mode peak for an as-cast film when heated from room temperature to 300 °C under inert atmosphere.[140] The initial peak position is at a high wavenumber (~1467 cm^{-1}) indicative of low molecular order, but upon heating to ~70 °C the peak shifts dramatically towards lower wavenumber (~1449 cm^{-1}) indicating a significant improvement in molecular order. This transition is associated with phase separation of the blend into purer, more crystalline domains, which is only possible at temperatures above the glass transition temperature, T_g, where the polymer chains become mobile. This transition is particularly significant, as the blend is considered to be morphologically stable below the lower limit of T_g. A second transition is observed at much higher temperatures, 180 °C - 220 °C, as the peak shifts back to high wavenumbers (greater disorder), corresponding with the melting point, T_m, of P3HT as measured by differential scanning calorimetry (~200 °C).[141] During subsequent cooling from 300 °C to 30 °C, the peak remained at higher wavenumbers until ~200 °C and a transition back to high molecular order was observed around 130 °C - 180 °C, indicating a crystallisation temperature (T_c) of ~151°C. Measurements of this kind provide a versatile probe for morphological changes and are particularly valuable for assessing temperature limits for stable device operation.[80] Combining *in situ* temperature dependent Raman spectroscopy with appropriate resonant excitation conditions (as discussed in Section 4.1) allows this technique to be used to monitor phase changes in multiple components of a blend film simultaneously.[120] However, the use of resonant excitation conditions also introduces the complexity of temperature-dependent resonant enhancement, since the strength and spectral position of the optical absorption bands show a temperature dependence.[142] Furthermore, significant optical absorption of the laser under resonant conditions may induce an additional localised heating effect, which must be accounted for.[143] For these reasons, a rigorously quantitative analysis of these data is a challenging aim, requiring further exploration.

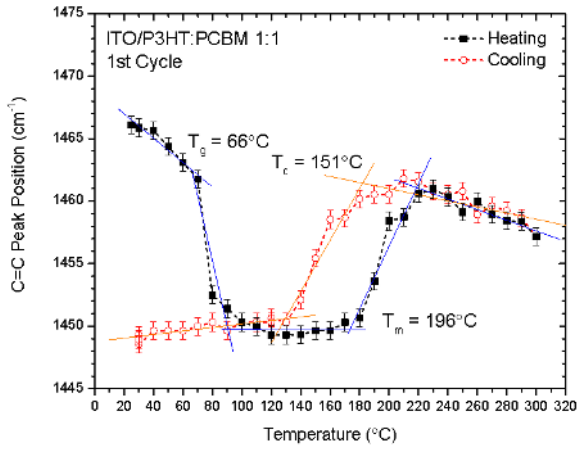

Figure 24. Plot showing peak position of main P3HT C=C Raman mode against temperature, measured for heating from room temperature to 300 °C followed by cooling, for a P3HT:PCBM blend film. Fit lines show extraction of glass (T_g), crystallisation (T_c), and melt (T_m) transition temperatures.[80]

This technique has also been extended to consider chemical strategies for improving morphological stability by increasing the phase transition temperatures. For conjugated polymers there is a close connection between backbone rigidity (and planarity) and morphological stability, such that highly planar polymers are expected to have higher transition temperatures. This has been explored for the case of fluorinated polythiophenes, using temperature-dependent Raman spectroscopy to probe the temperature at which the energetic barrier to rotation around the inter-unit C-C bond is overcome – in this case the more rigid fluorinated polymer was conformationally stable to a higher temperature than the non-fluorinated case.[87]

5.2. Photochemical Stability

5.2.1. Photostability of Conjugated Molecules

The sensitivity of Raman spectroscopy measurements to changes in chemical structure makes it an ideal technique for studying the photostability of organic semiconducting materials and identifying the mechanisms by which these molecules degrade. Photodegradation is a particular problem for some of the best-performing organic photovoltaic materials, since their operation requires prolonged exposure to intense sunlight. One polymer of particular interest is a donor-acceptor copolymer based on benzodithiophene and thienothiophene units (known as PTB7), which exhibits high power conversion efficiency (~ 9 %) but very limited operational lifetime when exposed to light and oxygen.[144] Insight into this photochemical degradation can be gained by comparing the Raman spectra of the material before and after exposure to air and simulated sunlight to examine the resulting changes in the chemical structure. Figure 25(a) illustrates the observed differences in the Raman spectra for the range 1450 cm^{-1} to 1600 cm^{-1}, corresponding with stretching modes of various carbon bonds in the conjugated backbone. The main peak, at 1489 cm^{-1} is found to shift towards higher wavenumber, and the relative intensities of the various peaks are also affected. These observations are interpreted using DFT calculations to simulate the effects of various possible oxidation products on the Raman spectrum (requiring a knowledge of related literature and some chemical intuition), and in this case, the closest match to the experimental data is found for hydroxylation of the aromatic C-H bonds on the benzodithiophene unit (see Figure 25(b)).[145]

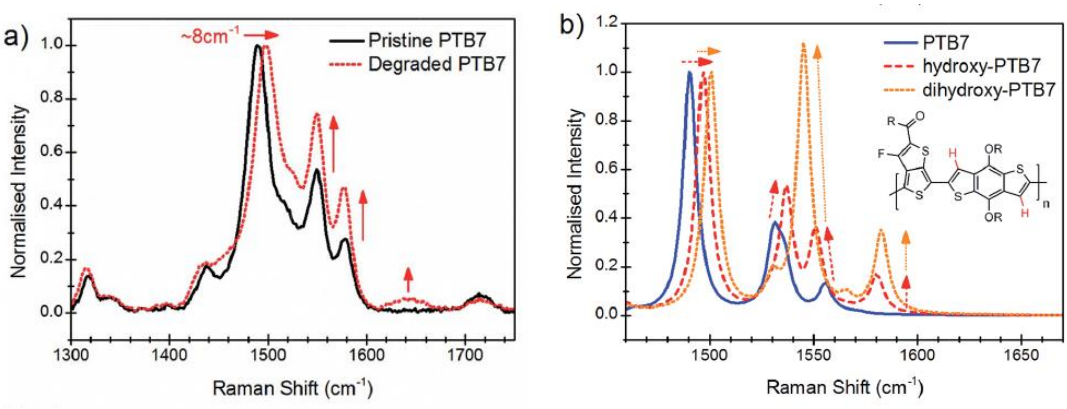

Figure 25. (a) Normalised Raman spectra measured for thin films of pristine and degraded PTB7, with red arrows indicating main changes due to degradation. (b) DFT calculated Raman activity spectra for PTB7 and prospective degradation products with single and double hydroxylation – inset chemical structure shows these additional hydrogen atoms in red.[145] *Adapted from J. Razzell-Hollis et al., Journal of Materials Chemistry C, 2, 20189, (2014), by permission of The Royal Society of Chemistry.*

Monitoring chemical changes in a sample during light exposure with Raman spectroscopy can be readily applied as an *in situ* technique provided the wavelength of the optical exposure (and any resulting emisssion or scattering) does not overlap strongly with the Raman scattering spectrum. A neat solution to this is to use a single (resonant) excitation wavelength to both induce photodegradation and simultaneously probe the resonant Raman spectrum. Figure 26 shows how the measured resonant Raman spectrum of PTB7 changes during exposure to optical excitation at 488 nm in air and in a nitrogen atmosphere. In this case the sample is found to be relatively stable in nitrogen, but when exposed to air, the Raman spectrum exhibits the changes associated with the hydroxylation described above followed by a total loss of Raman scattering intensity as the chromophore breaks down.[145]

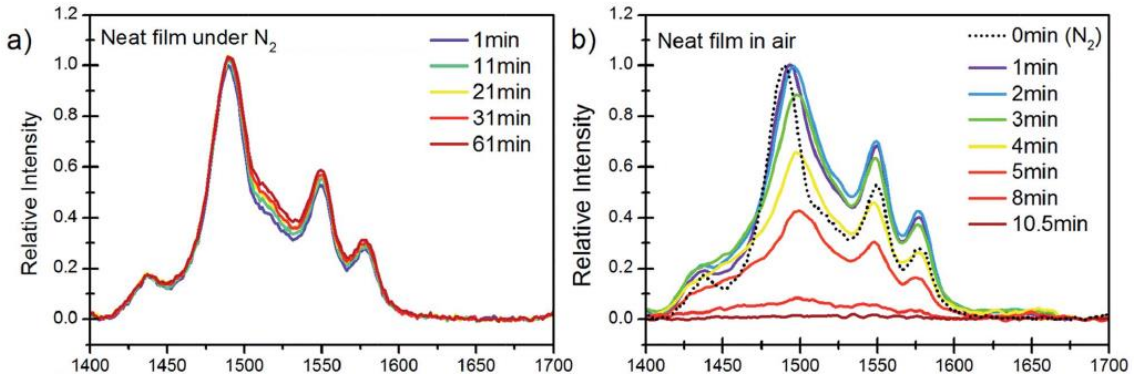

Figure 26. Resonant Raman spectra of neat PTB7 film during in situ *photodegradation under 488 nm excitation, measured (a) in nitrogen, and (b) in air. Spectra normalised to the initial intensity of the strongest peak.*[145] *Adapted from J. Razzell-Hollis et al., Journal of Materials Chemistry C, 2, 20189, (2014), by permission of The Royal Society of Chemistry.*

The photostability of conjugated molecules typically depends on the wavelength of the light exposure since different optically excited states can initiate different degradation pathways. By choosing appropriate laser excitation wavelengths to both activate and measure these degradation pathways using *in situ* resonant Raman spectoscopy, it is possible to identify the corresponding chemical changes and elucidate the different photodegradation mechanisms.[54] Care must be taken concerning the intensities and doses of the optical excitation with different wavelengths in order to make a meaningful comparison of photostabilities, and to avoid excessive heating or non-linear optical processes.

In some cases, photochemical reactions in conjugated molecule samples may be used as a processing step, such as the dimerisation of fullerenes for patterning or improving stability.[146,147] These dimers can be detected using chromatography or mass spectrometry, but Raman spectroscopy offers an alternative method for a quantitative measurement of dimerisation without destroying the sample. The $A_g(2)$ mode in C_{60} molecules is sensitive to changes in the electron density on the intramolecular conjugated bonds, such that the formation of intermolecular bonds by light-induced [2+2]-cycloaddition causes a shift in the spectral position of this peak from ~1464 cm^{-1} to lower wavenumbers when dimers form. Figure 27 illustrates this change in the measured Raman peak, where the degree of dimerisation can be calculated by fitting the peak with two Lorentzian functions representing the monomer and dimer contributions.[147]

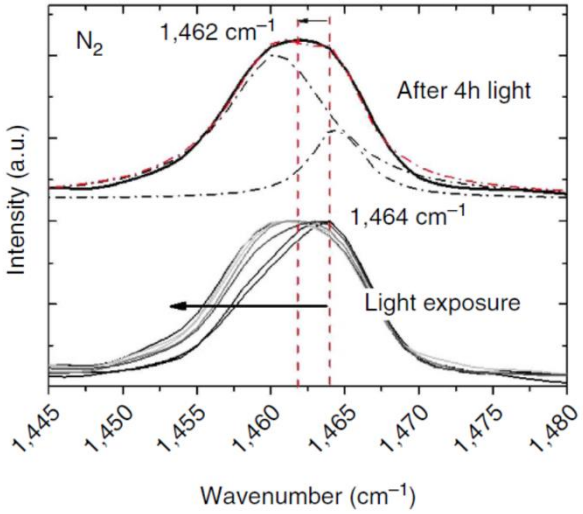

Figure 27. Detail of 1464 cm^{-1} Raman peak measured with 488 nm excitation for neat PCBM film showing effect of photoinduced dimerisation (top) before and after 4 hours of exposure to fluorescent light showing fitting with two Lorentzian functions, and (bottom) sequentially collected Raman spectra after 0, 10, 30, 50, 70, and 110 s of 488 nm laser exposure.[147] *Figure published previously in Z. Li et al., Nature Communications, 4, 2227, (2013).*

5.3. Electrochemical Raman Spectroscopy

The operation of molecular electronic devices can be described in terms of electrochemical processes, where electrical charges are transferred between molecules or redistributed within a system. For conjugated molecules, these effects relate primarily to the π-electron system to which Raman spectroscopy is particularly sensitive. The suitability of this technique has been demonstrated by a number of studies considering the doping of conjugated molecules, where the oxidised or reduced species are found to have distinct Raman spectra from the neutral state, associated with changes in the conformation of conjugated backbone. These charged species and the accompanying geometric distortion are often referred to as polarons. Polaronic states can be formed either through chemical or electrical doping.[148–152] Figure 28 compares the Raman spectra of neutral P3HT with chemically doped positive polarons and bipolarons (doubly charged species).[151]

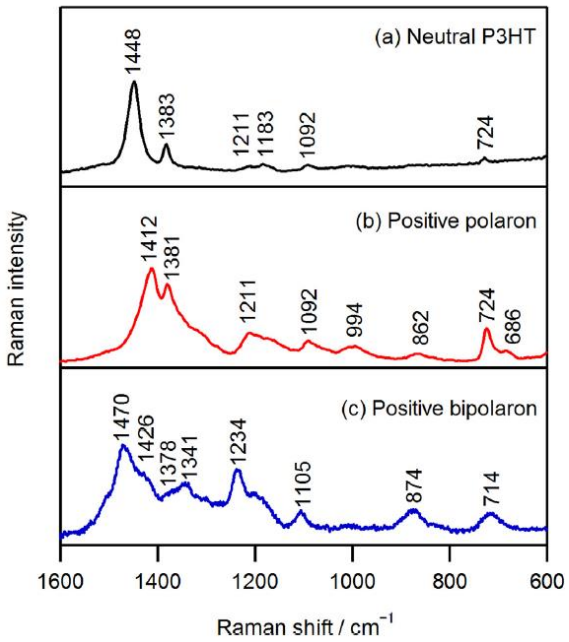

Figure 28. Comparison of Raman spectra for chemically doped P3HT with peak positions labelled for comparison: (a) neutral P3HT, (b) positive P3HT polaron, (c) positive P3HT bipolaron.[151] *Reprinted from J. Yamamoto and Y. Furukawa Organic Electronics, 28, 82, (2016). Copyright 2016, with permission from Elsevier.*

5.3.1. Electrochemical Degradation

In the previous Sections we have considered the degradation of organic semiconductors resulting from thermal and optical excitations, but electrochemical mechanisms are also found to impact the stability of these devices. In studies of polymer LEDs, Raman spectroscopy has been used to assign the formation of non-emissive spots to local de-doping of a common hole-injecting (PEDOT:PSS) layer associated with electrode pinhole defects.[153] Figure 29 shows Raman spectra measured for a similar study where the loss in performance of an LED device during accelerated testing was found to correlate with changes in the Raman spectrum. This effect was identified as an irreversible oxidation of the emissive polymer (PFB) by comparing the spectra measured *in situ* with reference spectra for neutral and chemically oxidised samples.[154]

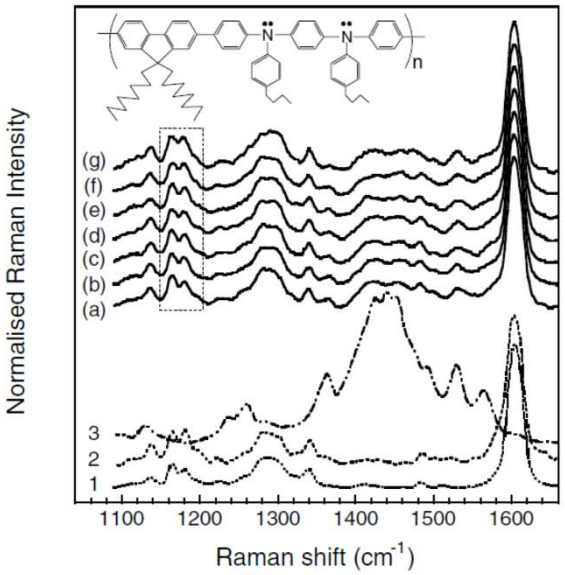

Figure 29. Raman spectra of an organic LED device with a PFB (structure shown) active layer: (a) to (f) show evolution of the measured spectrum during accelerated testing. Rectangle highlights spectral changes associated with PFB doping. Reference spectra below correspond with: (1) neat PFB, (2) oxidised PFB, (3) PEDOT:PSS hole-injection layer.[154] *Reprinted from J.-S. Kim et al., Chemical Physics Letters, 386, 2, (2004). Copyright 2004, with permission from Elsevier.*

More recently, the electrochemical stability of organic photovoltaic devices has also been considered, precipitated by the recognition that charged species may have an important role in the degradation pathways of operational solar cells.[155] In this case, comparison of Raman spectra measured for a polymer film before and after electrochemically induced degradation were compared to identify the chemical structural differences, and propose a mechanism for the observed change.[156]

5.3.2. Operational Studies of Electronic Devices

Characterisation of molecular semiconductor materials using *ex situ* and *in situ* measurements is able to reveal a great deal of information and insight into the properties and processes governing device performance, but the suspicion remains that the behaviour may be different under fully operational conditions. For this reason, spectroscopic measurements of devices during functional operation are attractive, and Raman spectroscopy is highly suitable. This sub-category of *in situ* measurement is sometimes, though not consistently, described as *operando* spectroscopy.

Several studies have detected changes in the Raman spectrum of conjugated semiconductors under applied bias in diode and transistor devices, however their observations and explanations are somewhat varied. In the case of pentacene transistors, the application of an electric field results in a partially irreversible change in the molecular packing structure, evidenced by changes in the relative intensities of the C-H bending and C-C aromatic stretching modes (exemplified by Figure 30) – this is a possible contributing factor to the 'bias stress' effect, where the electronic properties of a device change over time as a result of an applied bias.[157,158] A similar study considering conjugated polymer transistors found no differences in the Raman spectra of the active layer measured before and after biasing.[159]

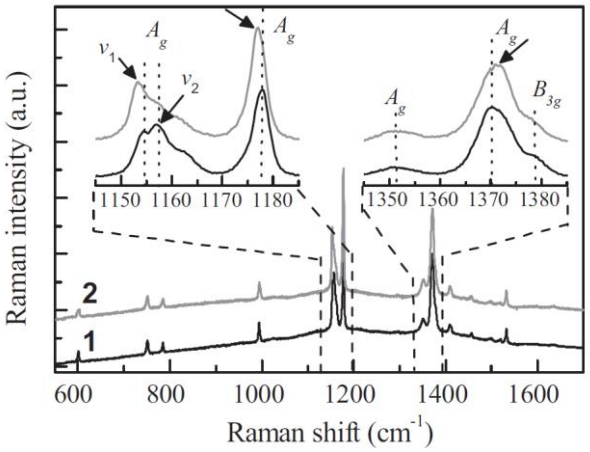

Figure 30. Comparison of Raman spectra measured for pentacene inside a transistor channel: (1) before operation, and (2) after 20 hours of device operation. Insets show detail for regions of interest.[158] *Reprinted with permission from H.L.L. Cheng et al., Advanced Functional Materials, 18, 285, (2008). Copyright 2008 WILEY-VCH Verlag GmbH & Co. KGaA, Weinheim.*

In addition to microstructural changes, Raman spectra of operational devices can also be used to identify and quantify the formation of polaronic states. In some studies the intensity of Raman scattering or the background signal is found to increase under applied bias, whereas others report changes in the shapes of the various peaks.[151,160,161] So far, there is not much consensus between different groups on the interpretations of these phenomena. In particular, care is required to distinguish effects arising from applied bias (gate bias and source-drain bias), applied current, light-induced effects, microstructural changes, and chemical degradation. Confocal spectroscopic mapping presents an exciting opportunity to map the polaron distribution in an organic semiconductor device, though published reports have had limited success.[161,162] It has been observed that polaron accumulation corresponds with a symmetry transformation of Raman active vibrational modes into IR active modes, such that IR absorption and Raman scattering spectroscopies are powerful complementary techniques in this instance. However, it also implies that the polaronic states have a lower Raman cross-section than the neutral species, which may explain some of the difficulty encountered in this type of measurement.[162,163]

6. Emerging Techniques

One of the main attractions of Raman spectroscopy for measurements such as those reviewed above, is the minimal sample preparation requirement and the relative ease of obtaining a measurement. However, there are a number of more complex emerging techniques that are beginning to find applications for characterisation of conjugated molecular semiconductors. Here we review a small number of these techniques that show particular promise.

6.1. Surface Enhanced Raman Spectroscopy (SERS)

Surface enhanced Raman spectroscopy (SERS) for organic semiconductors exploits electromagnetic surface plasmon resonances on metallic nanostructures, which produce a local enhancement of Raman scattering from molecules within a few nanometres of the metal surface. There is also a ‘chemical’ enhancement in Raman scattering observed for some systems, arising from electronic interactions between a molecule and a metal surface, but the ‘electromagnetic’ enhancement is typically dominant for molecular semiconductor samples.[164] Under certain conditions, Raman

scattering intensities can be dramatically increased by factors of up to 10^{11} by the surface enhancement.[165] This technique has been used extensively to detect and characterise trace molecules at extremely low concentrations, including single-molecule detection.[166,167]

Surface plasmons are oscillations of electron density localised at metal surfaces that can be resonantly excited by incident light with an appropriate frequency. For nanostructured metallic surfaces, the plasmonic excitation is confined, resulting in an intense evanescent electric field, which decays exponentially with distance (with an exponent as large as 12) from the metal surface and is spatially localised to around 10 nm.[168] Although several metals satisfy the requirements for surface plasmon resonance, silver and gold are the most commonly used for SERS, having resonance frequencies in the visible spectrum, strong evanescent fields and good chemical stability.

The intensity of Raman scattering from a molecule depends on the local electric field (E_{loc}). Therefore, those molecules within the near-field (in close proximity to the metal surface) exhibit enhanced Raman scattering compared with those in the un-enhanced far-field, E_0. In the simplest description, the intensity of Raman scattering produced by a molecule under SERS conditions (I_{SERS}, in the presence of metal) is enhanced compared to its normal Raman scattering (I_{RS}, in the absence of metal) by the enhancement factor, *EF*, which is given by the $|E|^4$ approximation in Equation 13.[168]

$$EF = \frac{I_{SERS}}{I_{RS}} \approx \frac{|E_{loc}(\omega_0)|^4}{|E_0|^4} \qquad (13)$$

This expression reveals that a relatively small increase in local electric field can result in a large *EF*. The sensitivity of electric field to local geometry leads to 'hot spots' of particularly high *EF*, such as at the corners of triangular structures, at the point of a metal-coated AFM tip, or in the narrow gap between two nanoparticles. As a result, a high degree of control over the metal nanostructure is required for quantitative analysis.

More detailed reviews of the theory behind the SERS effect are available elsewhere, but here we focus specifically on the application to organic semiconductors.[164,169,170] For these applications, the spatial localisation of the SERS effect is of particular interest, since it can be exploited to selectively probe molecules at the metal-organic interface. These interfaces play a significant role in device operation, as the location of charge injection or extraction in OLEDs and OPVs respectively, so it is important to characterise how the interfacial properties differ from those of the bulk film. Figure 31 compares Raman spectra for a ~100 nm thick conjugated polymer (MEH-PPV) film deposited on glass, silver, and gold surfaces where the differences in the measured spectra are assigned to the different conformations and orientations of the polymer molecules within the surface-enhanced region at the organic-metal interface.[171]

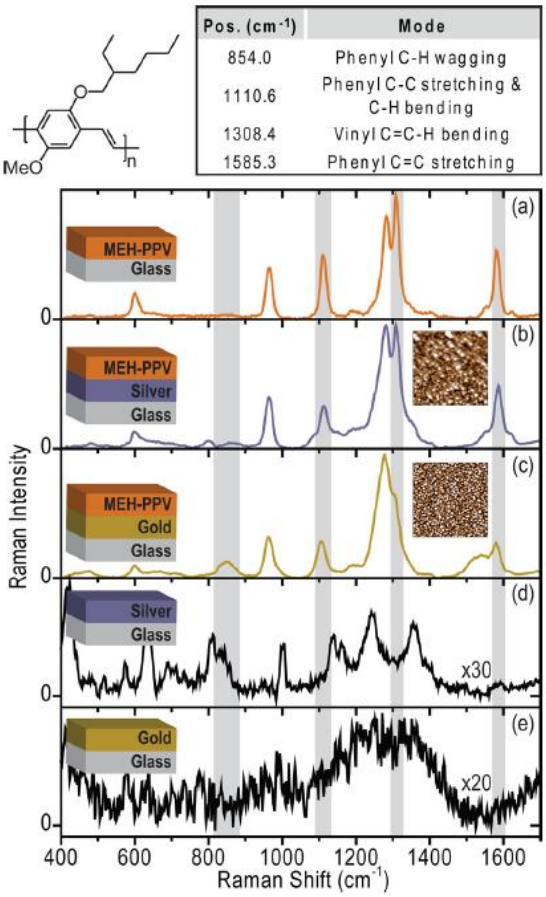

Figure 31. Raman spectra of MEH-PPV (chemical structure shown) for various sample structures, highlighting important vibrational modes: (a) bulk MEH-PPV, (b) MEH-PPV on silver film, (c) MEH-PPV on gold film. Insets show surface topographies for uncoated silver and gold films with lateral scale 1 µm × 1 µm, and height scales: 10 nm and 6 nm, respectively. (d) and (e) show background signals for the silver and gold films, respectively.[171] *Reprinted from D. Li et al., Applied Physics Letters, 100, 141907, (2012), with the permission of AIP Publishing.*

The localised enhancement at the organic-metal interface can also be used to measure the interfacial chemical composition of a blended organic semiconductor films. By depositing the blend film on a nanostructured gold surface, the relative intensities of the surface-enhanced Raman scattering peaks for the different materials provide a measure of the composition at the interface. The length scale of the enhancement effect, corresponding with the vertical resolution of the measurement, was measured at around 20 nm by using bilayer reference samples.[172]

The use of SERS in the study of organic semiconductors to date is limited, perhaps because of the complexity of the measurements and the difficulty in ensuring that any observations are representative. One such difficulty is that the nanostructured metal interacts with the organic material and so can interfere with the morphology being probed.[171] Care must also be taken to find an appropriate excitation wavelength that is both in resonance with the surface plasmon mode and suitable for probing the intended organic material. A further issue is that although EF values can be calculated for monolayers with a known number of molecules, it is much harder to accurately define or determine EF for thicker polymer films, where the number of molecules (or chromophores

undergoing Raman scattering) is not known and absorption by the different layers may need to be accounted for to obtain accurate intensity values in different sample configurations.

With this in mind, the goal of using SERS to quantitatively measure interfacial composition and other device-critical properties, like molecular orientation, requires more work understanding the fundamentals of its application to organic semiconductor devices. However, the published results to date have demonstrated the potential of this advanced technique for selectively probing interfacial properties.[170,171,173]

6.2. Tip-Enhanced Raman Spectroscopy (TERS)

While SERS provides surface sensitivity with nanometric vertical resolution,[174] it is possible to extend to technique for laterally resolved mapping with comparable resolution by localising the plasmonic field enhancement onto the tip of a scanning probe microscopy (SPM) cantilever; this technique is known as tip-enhanced Raman spectroscopy (TERS), and is schematically represented in Figure 32. The plasmonic enhancement can be achieved by coating an SPM tip with a suitable metal (typically silver or gold). By bringing this tip near to a sample surface, and focusing a laser beam on it to excite the plasmonic resonance, it is possible to enhance the Raman scattering from the region close to the tip apex by factors of up to 10^8.[175] In this way, spatially resolved Raman spectroscopy can be achieved with resolution exceeding the diffraction limit (better than 10 nm resolution has been reported in some cases).[176]

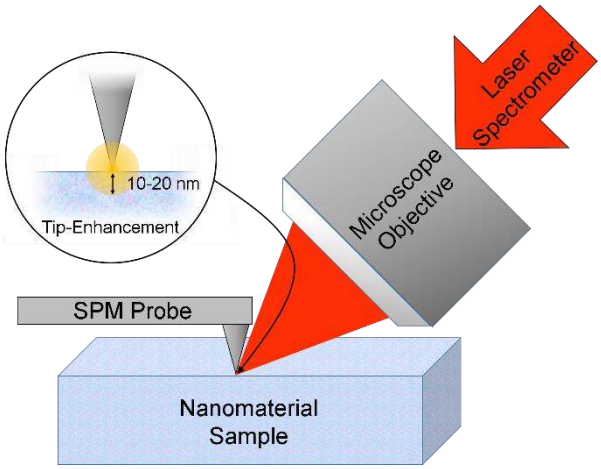

Figure 32. Schematic diagram indicating measurement geometry for side-illumination tip-enhanced Raman spectroscopy.

In practice, TERS measurements remain experimentally challenging, but have been successfully employed across a broad range of research fields.[176,177] To date, however, there are very few reports related to conjugated molecular semiconductor applications, most notably a contribution by Wang *et al.* who demonstrated high-resolution spectroscopic mapping of annealed P3HT:PCBM blends – see Figure 33.[178,179] These blends are known to phase-separate during thermal annealing, with diffusion leading to nanoscale domains rich in either P3HT or PCBM. Tip-enhanced spectroscopy was used to simultaneously measure the Raman scattering, photoluminescence emission, and surface topography with a lateral resolution of approximately 10nm. This resolution is particularly relevant to organic photovoltaics because it is roughly equal to the exciton diffusion length that defines an optimum domain size for efficient photocurrent generation.[26] In this study

of P3HT:PCBM blends annealed at 140 °C for either 5 minutes or 30 minutes, PCBM-rich islands were detected on the film surface with diameters < 100 nm after 5 min and ~300 nm after 30 min of annealing, demonstrating the progression of phase separation over time at this temperature. Interestingly, the maps revealed a homogenous distribution of P3HT across the whole surface, including the PCBM-rich island. In this example, the greatest optical contrast was actually obtained from differences in the photoluminescence (PL), indicating variations in chemical composition and the degree of intermixing (evident from the PL quenching).[179]

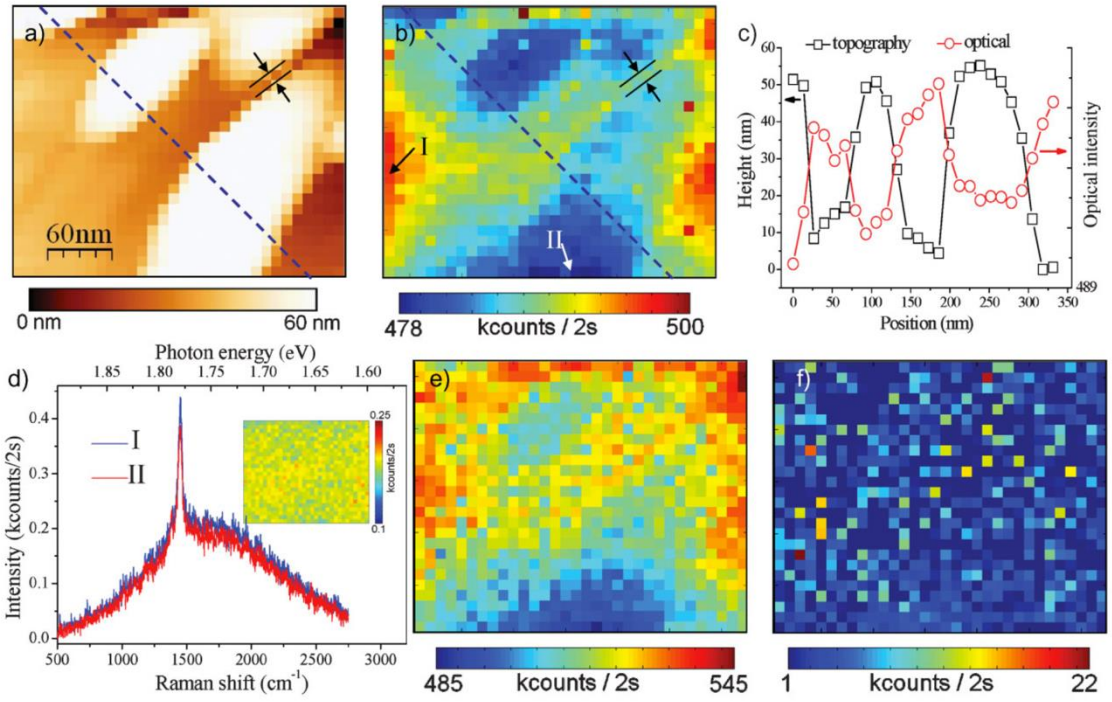

Figure 33. (a) Surface topography, and (b) Integrated near-field optical intensity images of the P3HT:PCBM sample annealed at 140 °C for 5 min. (c) Comparison of topography and optical intensity profiles along the dashed line in (a) and (b). (d) Tip-enhanced Raman spectra collected at positions I and II in (b), inset shows Raman intensity map of main C=C mode of P3HT. Photoluminescence intensity maps of (e) P3HT, and (f) PCBM.[179] *Reprinted with permission from X. Wang et al., Advanced Functional Materials, 20, 492, (2010). Copyright 2010 WILEY-VCH Verlag GmbH & Co. KGaA, Weinheim.*

As with SERS, TERS has so far had limited application to the study of organic semiconductors but has the potential to be a powerful tool, providing both signal enhancement and high spatial resolution that are key to characterising nanoscale morphology. Combined with the various capabilities of Raman spectroscopy (reviewed above) for studies of many different properties of conjugated molecular semiconductors, from chemical composition to molecular conformation, TERS could be used to investigate the nanoscale distribution of these properties throughout organic thin films and inform the optimisation of device fabrication towards better morphologies for high-performance devices.

6.3. Non-Linear Raman Spectroscopy

The experimental techniques used for the studies described so far all make use of spontaneous Raman scattering, the magnitude of which is linear with respect to the excitation intensity. However,

many other types of Raman spectroscopy have been developed based on the non-linear, stimulated Raman effect. To date, the application of these techniques to conjugated molecular semiconductors is limited and primarily concerned with fundamental molecular properties that lie outside the scope of this Review, but it is appropriate to acknowledge their existence and contribution to the subject.

Spontaneous Raman scattering arises when a molecule is optically excited with a pump wavelength and the scattered light is detected at a different (anti-)Stokes wavelength. In stimulated Raman spectroscopy (SRS), two beams are incident on the molecule with pump and Stokes wavelengths respectively. If the differences between these wavelengths matches the energy of a Raman-active vibrational mode, energy is transferred between the two optical fields resulting in a loss in the pump-field intensity and a gain in the Stokes-field intensity. The primary advantage of SRS over spontaneous Raman spectroscopy is that the Raman signal is much stronger and so measurements are faster and more sensitive. This makes SRS, and other coherent Raman scattering processes, such as coherent anti-stokes Raman scattering (CARS), particularly useful for imaging of biological samples.[180]

Many related non-linear Raman spectoscopy techniques exist, but one of particular interest is femtosecond stimulated Raman spectroscopy (FSRS), which is capable of making ultrafast time-resolved measurements of molecular processes.[181,182] This is particularly relevant for organic photovoltaics, where the charge generation mechanism occurs on this timescale and is not yet fully understood. Provencher *et al.* were able to probe this process directly in a polymer:fullerene (PCDTBT:PCBM) blend film using FSRS.[183] This measurement requires three pulses to overlap spatially and temporally within the sample: a femtosecond actinic pump to initiate the photochemistry; a picosecond Raman pump; and a broadband femtosecond probe. Time resolution below 100 fs is gained by controlling the delay between the actinic and probe pulses. The gain on the probe pulse corresponds with the Raman spectrum of the excited sample.

Figure 34 shows the absorption spectra of neat PCDTBT with the PCDTBT:PCBM blend films and that of doped PCDTBT. The actinic pulse wavelength is chosen to photoexcite the neutral polymer, whereas the Raman pump wavelength is chosen to match the peak of the photoinduced absorption related to the polaronic state. Comparison of the Raman spectra of the neutral and doped polymer show clear differences in the relative peak intensities and shapes by which the two states can be distinguished. Comparison of these peak intensities for time resolved measurements provides a means of tracking the populations of the excitonic and polaronic states during the photogeneration of charge, and gives some insight into the mechanism itself. In this case, charge generation occurs faster (< 300 fs) than localisation of the exciton (~3 ps), which might explain the high photovoltaic performance of this material system.

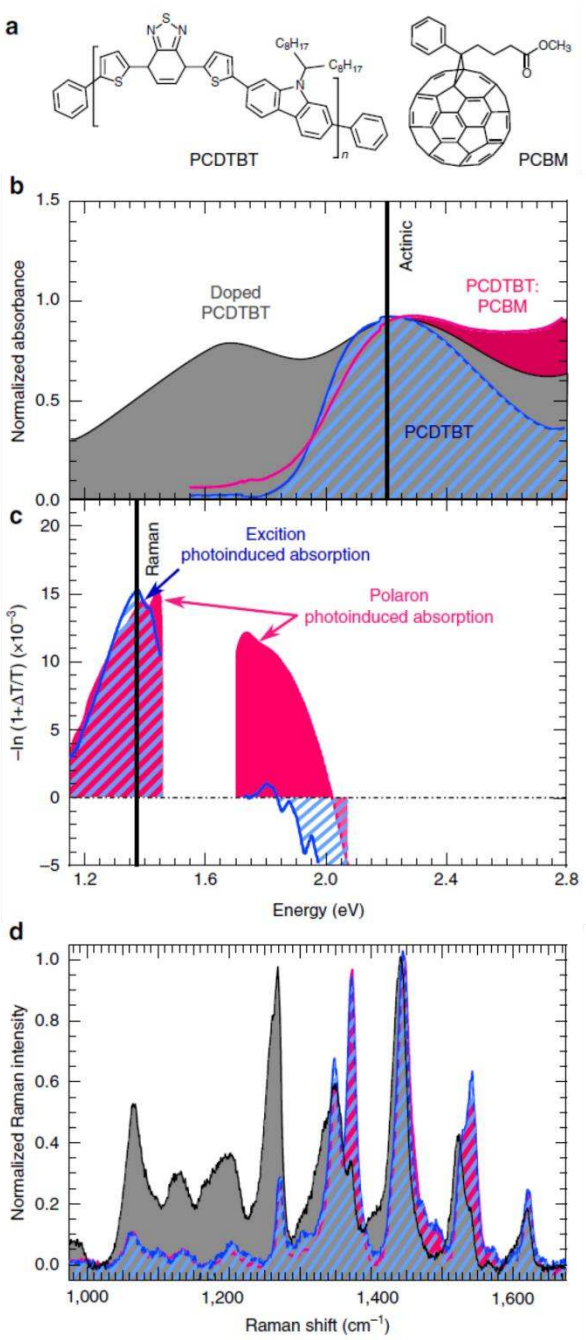

Figure 34. (a) Chemical structures of PCDTBT and PCBM. (b) Absorption spectra, (c) transient absorption spectra, and (d) resonant Raman spectra of neat PCDTBT (blue), PCDTBT:PCBM (pink), and doped PCDTBT (grey) thin films. Spectral positions of actinic and Raman pulses indicated by vertical lines.[183] *Reprinted by permission from Macmillan Publishers Ltd: Nature Communications F. Provencher et al., 5, 4288, (2014), copyright 2014.*

7. Conclusion and Outlook

The study of conjugated molecular semiconductors, and the development of organic electronics more generally, is dependent upon a clear understanding of the relationship between molecular structure and solid state optoelectronic properties. Gaining insight into these complex relationships challenges the capabilities of established characterisation techniques, and requires the development of suitable experimental methods for probing their nanoscale structure and related properties. As

we have seen, Raman spectroscopy is well-suited for this type of measurement in a wide variety of contexts.

In addition to the capabilities of Raman spectroscopy, we have also noted some specific challenges to be overcome in the development of these techniques. Much of the published work reviewed above is comparative in nature, whereas fully quantitative measurements are preferable in order to make comparisons between different laboratories and instruments. Progress in this regard requires not only developments in experiment design, but also the identification of appropriate reference samples. Other limitations, in terms of spatial and temporal resolution are already being addressed with emerging techniques, which indicate the future trajectory of Raman spectroscopy. The application of these techniques to molecular semiconductors remains in its infancy, but they offer a way to probe functionally important, and otherwise inaccessible, time and length scales.

In summary, Raman spectroscopy offers an enormously versatile and sensitive technique, capable of providing uniquely detailed insights that have had a demonstrable impact on the development of organic semiconductor devices. The continued development of stable, high-performance molecular electronics is critically reliant on suitable characterisation techniques, among which, Raman spectroscopy is uniquely powerful.

We acknowledge the EPSRC support through the Plastic Electronics Centre for Doctoral Training (EP/L016702/1) and Research grant (EP/K029843/1).

8. References

[1] Moliton A and Hiorns R C 2012 The origin and development of (plastic) organic electronics *Polym. Int.* **61** 337–41

[2] Ratner M 2013 A brief history of molecular electronics *Nat. Nanotechnol.* **8** 378–81

[3] Pope M and Swenberg C E 1999 *Electronic Processes in Organic Crystals and Polymers* (Oxford: Oxford University Press)

[4] Arias A C, MacKenzie J D, McCulloch I, Rivnay J and Salleo A 2010 Materials and applications for large area electronics: Solution-based approaches *Chem. Rev.* **110** 3–24

[5] Po R, Bernardi A, Calabrese A, Carbonera C, Corso G and Pellegrino A 2014 From lab to fab: how must the polymer solar cell materials design change? – an industrial perspective *Energy Environ. Sci.* **7** 925–43

[6] Ferrari A C 2007 Raman spectroscopy of graphene and graphite: Disorder, electron-phonon coupling, doping and nonadiabatic effects *Solid State Commun.* **143** 47–57

[7] Dresselhaus M S, Jorio A and Saito R 2010 Characterizing Graphene, Graphite, and Carbon Nanotubes by Raman Spectroscopy *Annu. Rev. Condens. Matter Phys* **1** 89–108

[8] Brütting W 2005 Introduction to the Physics of Organic Semiconductors *Physics of Organic Semiconductors* ed W Brütting (Weinheim, FRG: Wiley-VCH Verlag GmbH & Co. KGaA) pp 1–14

[9] Dyer-Smith C and Nelson J 2005 Organic Solar Cells *Solar Cells: Materials, Manufacture & Operation* ed T Markvart and L Castaner (Oxford: Elsevier) pp 443–66

[10] Jou J-H, Kumar S, Agrawal A, Li T-H and Sahoo S 2015 Approaches for fabricating high

efficiency organic light emitting diodes *J. Mater. Chem. C* **3** 2974–3002

[11] Dou L, You J, Hong Z, Xu Z, Li G, Street R A and Yang Y 2013 25th Anniversary Article: A Decade of Organic/Polymeric Photovoltaic Research *Adv. Mater.* **25** 6642–71

[12] Lin P and Yan F 2012 Organic Thin-Film Transistors for Chemical and Biological Sensing *Adv. Mater.* **24** 34–51

[13] Sirringhaus H 2014 25th Anniversary Article: Organic Field-Effect Transistors: The Path Beyond Amorphous Silicon *Adv. Mater.* **26** 1319–35

[14] Coropceanu V, Cornil J, da Silva Filho D A, Olivier Y, Silbey R and Brédas J-L 2007 Charge Transport in Organic Semiconductors *Chem. Rev.* **107** 926–52

[15] Takeda Y, Hayasaka K, Shiwaku R, Yokosawa K and Shiba T 2016 Fabrication of Ultra-Thin Printed Organic TFT CMOS Logic Circuits Optimized for Low-Voltage Wearable Sensor Applications *Sci. Rep.* **6** 25714

[16] Yi Z, Wang S and Liu Y 2015 Design of High-Mobility Diketopyrrolopyrrole-Based π-Conjugated Copolymers for Organic Thin-Film Transistors *Adv. Mater.* **27** 3589–606

[17] Kang C, Wade J, Yun S, Lim J, Cho H, Roh J, Lee H, Nam S, Bradley D D C, Kim J-S and Lee C 2015 1 GHz Pentacene Diode Rectifiers Enabled by Controlled Film Deposition on SAM-Treated Au Anodes *Adv. Electron. Mater.* **2** 1500282

[18] Qian Y, Zhang X, Xie L, Qi D, Chandran B K, Chen X and Huang W 2016 Stretchable Organic Semiconductor Devices *Adv. Mater.* doi:10.1002/adma.201601278

[19] Meier S B, Tordera D, Pertegás A, Roldán-Carmona C, Ortí E and Bolink H J 2014 Light-emitting electrochemical cells: Recent progress and future prospects *Mater. Today* **17** 217–23

[20] Peng B, Ren X, Wang Z, Wang X, Roberts R C and Chan P K L 2014 High performance organic transistor active-matrix driver developed on paper substrate *Sci. Rep.* **4** 6430

[21] Fukuda K, Takeda Y, Mizukami M, Kumaki D and Tokito S 2014 Fully solution-processed flexible organic thin film transistor arrays with high mobility and exceptional uniformity. *Sci. Rep.* **4** 3947

[22] Few S, Frost J M and Nelson J 2015 Models of Charge Pair Generation in Organic Solar Cells *Phys. Chem. Chem. Phys.* **17** 2311–25

[23] Gao F and Inganäs O 2014 Charge generation in polymer-fullerene bulk-heterojunction solar cells. *Phys. Chem. Chem. Phys.* **16** 20291–304

[24] Halls J J M, Pichler K and Friend R H 1996 Exciton diffusion and dissociation in a poly (p-phenylenevinylene)/C60 heterojunction photovoltaic cell *Appl. Phys. Lett.* **68** 3120–2

[25] Treat N D, Brady M A, Smith G, Toney M F, Kramer E J, Hawker C J and Chabinyc M L 2011 Interdiffusion of PCBM and P3HT Reveals Miscibility in a Photovoltaically Active Blend *Adv. Energy Mater.* **1** 82–9

[26] Shaw P E, Ruseckas A and Samuel I D W 2008 Exciton Diffusion Measurements in Poly(3-hexylthiophene) *Adv. Mater.* **20** 3516–20

[27] Gevorgyan S A, Madsen M V., Roth B, Corazza M, Hösel M, Søndergaard R R, Jørgensen M and Krebs F C 2015 Lifetime of Organic Photovoltaics: Status and Predictions *Adv. Energy*

Mater. 1–17

[28] Savagatrup S, Printz A D, O'Connor T F, Zaretski A V., Rodriquez D, Sawyer E J, Rajan K M, Acosta R I, Root S E and Lipomi D J 2014 Mechanical degradation and stability of organic solar cells: molecular and microstructural determinants *Energy Environ. Sci.* **8** 55–80

[29] Cheng P and Zhan X 2016 Stability of organic solar cells: challenges and strategies *Chem. Soc. Rev.* **45** 2544

[30] Huang Y, Kramer E J, Heeger A J and Bazan G C 2014 Bulk heterojunction solar cells: morphology and performance relationships. *Chem. Rev.* **114** 7006–43

[31] Diao Y, Shaw L and Mannsfeld S C B 2014 Morphology control strategies for solution-processed organic semiconductor thin fi lms *Energy Environ. Sci.* **7** 2145–59

[32] James D T, Frost J M, Wade J, Nelson J and Kim J 2013 Controlling Microstructure of Pentacene Derivatives by Solution Processing : Impact of Structural Anisotropy on Optoelectronic Properties *ACS Nano* **7** 7983–91

[33] Wade J, Steiner F, Niedzialek D, James D T, Jung Y, Yun D-J, Bradley D D C, Nelson J and Kim J 2014 Charge mobility anisotropy of functionalized Pentacenes in organic field effect transistors farbicated by solution processing *J. Mater. Chem. C* **2** 10110–5

[34] Noriega R, Rivnay J, Vandewal K, Koch F P V, Stingelin N, Smith P, Toney M F and Salleo A 2013 A general relationship between disorder, aggregation and charge transport in conjugated polymers. *Nat. Mater.* **12** 1038–44

[35] Niazi M R, Li R, Li E Q, Kirmani A R, Abdelsamie M, Wang Q, Pan W, Payne M M, Anthony J E, Smilgies D-M, Thoroddsen S T, Giannelis E P and Amassian A 2015 Solution-printed organic semiconductor blends exhibiting transport properties on par with single crystals *Nat. Commun.* **6** 8598

[36] Lu L, Kelly M A, You W and Yu L 2015 Status and prospects for ternary organic photovoltaics *Nat. Photonics* **9** 491–500

[37] Ferenczi T A M, Müller C, Bradley D D C, Smith P, Nelson J and Stingelin N 2011 Organic semiconductor: Insulator polymer ternary blends for photovoltaics *Adv. Mater.* **23** 4093–7

[38] Hellmann C, Treat N D, Scaccabarozzi A D, Razzell Hollis J, Fleischli F D, Bannock J H, de Mello J, Michels J J, Kim J-S and Stingelin N 2015 Solution processing of polymer semiconductor: Insulator blends-Tailored optical properties through liquid-liquid phase separation control *J. Polym. Sci. Part B Polym. Phys.* **53** 304–10

[39] Shao W, Dong H L, Jiang L and Hu W P 2011 Morphology control for high performance organic thin film transistors *Chem. Sci.* **2** 590–600

[40] Westacott P, Tumbleston J R, Shoaee S, Fearn S, Bannock J H, Gilchrist J B, Heutz S, de Mello J, Heeney M, Ade H, Durrant J, McPhail D S and Stingelin N 2013 On the role of intermixed phases in organic photovoltaic blends *Energy Environ. Sci.* **6** 2756–64

[41] Bartelt J A, Beiley Z M, Hoke E T, Mateker W R, Douglas J D, Collins B A, Tumbleston J R, Graham K R, Amassian A, Ade H, Fréchet J M J, Toney M F and McGehee M D 2013 The Importance of Fullerene Percolation in the Mixed Regions of Polymer-Fullerene Bulk Heterojunction Solar Cells *Adv. Energy Mater.* **3** 364–74

[42] Scarongella M, Paraecattil A A, Buchaca-Domingo E, Douglas J D, Beaupré S, McCarthy-Ward T, Heeney M, Moser J-E, Leclerc M, Fréchet J M J, Stingelin N and Banerji N 2014 The influence of microstructure on charge separation dynamics in organic bulk heterojunction materials for solar cell applications *J. Mater. Chem. A* **2** 6218

[43] Steim R, Kogler F R and Brabec C J 2010 Interface materials for organic solar cells *J. Mater. Chem.* **20** 2499–512

[44] Don Park Y, Lim J A, Lee H S and Cho K 2007 Interface engineering in organic transistors *Mater. Today* **10** 46–54

[45] Jørgensen M, Norrman K, Gevorgyan S A, Tromholt T, Andreasen B and Krebs F C 2012 Stability of polymer solar cells. *Adv. Mater.* **24** 580–612

[46] Salleo A, Kline R J, DeLongchamp D M and Chabinyc M L 2010 Microstructural characterization and charge transport in thin films of conjugated polymers. *Adv. Mater.* **22** 3812–38

[47] Chen W, Nikiforov M P and Darling S B 2012 Morphology characterization in organic and hybrid solar cells *Energy Environ. Sci.* **5** 8045

[48] Paternò G, Warren A J, Spencer J, Evans G, Sakai V G, Blumberger J and Cacialli F 2013 Micro-focused X-ray diffraction characterization of high-quality [6,6]-phenyl-C61-butyric acid methyl ester single crystals without solvent impurities *J. Mater. Chem. C* **1** 5619

[49] DeLongchamp D M, Kline R J and Herzing A 2012 Nanoscale structure measurements for polymer-fullerene photovoltaics *Energy Environ. Sci.* **5** 5980–93

[50] van Bavel S S, Sourty E, de With G and Loos J 2009 Three-Dimensional Nanoscale Organization of Bulk Heterojunction Polymer Solar Cells *Nano Lett.* **9** 507–13

[51] Nicholson P G and Castro F A 2010 Organic photovoltaics: principles and techniques for nanometre scale characterization. *Nanotechnology* **21** 492001

[52] Köhler A and Bässler H 2015 *Electronic Processes in Organic Semiconductors: An Introduction* (John Wiley & Sons)

[53] Myers Kelley A 2013 *Condensed-Phase Molecular Spectroscopy and Photophysics* (Hoboken, New Jersey: John Wiley & Sons)

[54] Wood S, Wade J, Shahid M, Collado Fregoso E, Bradley D D C, Durrant J, Heeney M and Kim J-S 2015 Natures of Optical Absorption Transitions and Excitation Energy Dependent Photostability of Diketopyrrolopyrrole (DPP)-Based Photovoltaic Copolymers *Energy Environ. Sci.* **8** 3222–32

[55] Long D A 2002 *The Raman Effect* (Chichester, UK: John Wiley & Sons, Ltd)

[56] Smith E and Dent G 2005 *Modern Raman Spectroscopy – A Practical Approach* (Chichester, UK: John Wiley & Sons, Ltd)

[57] Ferraro J R, Nakamoto K and Chris W Brown 2003 *Introductory Raman Spectroscopy* (San Diego: Academic Press)

[58] Amer M S 2010 *Raman Spectroscopy, Fullerenes and Nanotechnology* ed P O'Brien, H Kroto and H Craighead (Cambridge, UK: Royal Society of Chemistry)

[59] Rousseau D L, Friedman J M and Williams P F 1979 The Resonance Raman Effect *Top. Curr. Phys.* **2** 203

[60] Myers A B and Mathies R A 1987 Resonance Raman Intensities: A Probe of Excited-State Structure and Dynamics *Biological Applications of Raman Spectroscopy* ed T G Spiro (New York: Wiley) pp 1–58

[61] Castiglioni C, Del Zoppo M and Zerbi G 1993 Vibrational Raman Spectroscopy of Polyconjugated Organic Oligomers and Polymers *J. Raman Spectrosc.* **24** 485–94

[62] Castiglioni C, Tommasini M and Zerbi G 2004 Raman spectroscopy of polyconjugated molecules and materials: confinement effect in one and two dimensions. *Phil. Trans. R. Soc. Lond. A* **362** 2425–59

[63] Brivio G P and Mulazzi E 1983 Absorption and Resonant Raman Scattering from Trans-(CH)x *Chem. Phys. Lett.* **95** 555–60

[64] Shand M L, Chance R R, LePostollec M and Schott M 1982 Raman photoselection and conjugation-length dispersion in conjugated polymer solutions *Phys. Rev. B* **25** 4431

[65] Ehrenfreund E, Vardeny Z and Brafman O 1987 Amplitude and phase modes in trans-polyacetylene: Resonant Raman scattering and induced infrared activity *Phys. Rev. B* **36** 1535

[66] Vardeny Z, Ehrenfreund E, Brafman O and Horovitz B 1983 Resonant Raman Scattering from Amplitude Modes in trans-(CH)x and -(CD)x *Phys. Rev. Lett.* **51**

[67] Castiglioni C, Lopez Navarrete J T, Zerbi G and Gussoni M 1988 A simple interpretation of the vibrational spectra of undoped, doped and photoexcited polyacetylene amplitude mode theory in the GF formalism *Solid State Commun.* **65** 625–30

[68] Lopez-Navarrete J T, Tian B and Zerbi G 1990 Relation between effective conjugation, vibrational force constants and electronic properties in polyconjugated materials *Solid State Commun.* **74** 199–202

[69] Tian B, Zerbi G and Müllen K 1991 Electronic and structural properties of polyparaphenylenevinylene from the vibrational spectra *J. Chem. Phys.* **95** 3198

[70] Agosti E, Rivola M, Hernandez V, Del Zoppo M and Zerbi G 1999 Electronic and dynamical effects from the unusual features of the Raman spectra of oligo and polythiophenes *Synth. Met.* **100** 101–12

[71] Schaffer H E, Chance R R, Silbey R J, Knoll K and Schrock R R 1991 Conjugation length dependence of Raman scattering in a series of linear polyenes: Implications for polyacetylene *J. Chem. Phys.* **94** 4161–70

[72] Lin-Vien D, Colthup N B, Fateley W G and Grasselli J G 1991 *The Handbook of Infrared and Raman Characteristic Frequencies of Organic Molecules* (San Diego: Academic Press)

[73] Schettino V, Gervasio F L, Cardini G and Salvi P R 1999 Density functional calculation of structure and vibrational spectra of polyenes *J. Chem. Phys.* **110** 3241–50

[74] Bianco A, Del Zoppo M and Zerbi G 2004 Experimental CC stretching phonon dispersion curves and electron phonon coupling in polyene derivatives *J. Chem. Phys.* **120** 1450–7

[75] Jensen L and Schatz G C 2006 Resonance Raman scattering of rhodamine 6G as calculated using time-dependent density functional theory. *J. Phys. Chem. A* **110** 5973–7

[76] Tanaka M and Young R J 2006 Review Polarised Raman spectroscopy for the study of molecular orientation distributions in polymers *J. Mater. Sci.* **41** 963–91

[77] Roy S, Hung K-K, Stege U and Hore D K 2013 Rotations, Projections, Direction Cosines, and Vibrational Spectra *Appl. Spectrosc. Rev.* **49** 233–48

[78] McCreery R L 2000 *Raman Spectroscopy for Chemical Analysis* ed J D Winefordner (New York: John Wiley & Sons)

[79] Tsoi W C, Spencer S J, Yang L, Ballantyne A M, Nicholson P G, Turnbull A, Shard A G, Murphy C E, Bradley D D C, Nelson J and Kim J-S 2011 Effect of Crystallization on the Electronic Energy Levels and Thin Film Morphology of P3HT:PCBM Blends *Macromolecules* **44** 2944–52

[80] Razzell Hollis J, Limbu S and Kim J 2016 Spectroscopic Investigations of Three-Phase Morphology Evolution in Polymer: Fullerene Solar Cell Blends *J. Phys. Chem. C* **120** 10806

[81] Becker M, Scheel H, Christiansen S and Strunk H P 2007 Grain orientation, texture, and internal stress optically evaluated by micro-Raman spectroscopy *J. Appl. Phys.* **101** 63531

[82] Shao M, Keum J, Chen J, He Y, Chen W, Browning J F, Jakowski J, Sumpter B G, Ivanov I N, Ma Y-Z, Rouleau C M, Smith S C, Geohegan D B, Hong K and Xiao K 2014 The isotopic effects of deuteration on optoelectronic properties of conducting polymers. *Nat. Commun.* **5** 3180

[83] Ballantyne A M, Ferenczi T A M, Campoy-Quiles M, Clarke T M, Maurano A, Wong K H, Zhang W, Stingelin-Stutzmann N, Kim J-S, Bradley D D C, Durrant J R, McCulloch I, Heeney M, Nelson J, Tierney S, Duffy W, Mueller C and Smith P 2010 Understanding the Influence of Morphology on Poly(3-hexylselenothiophene):PCBM Solar Cells *Macromolecules* **43** 1169–74

[84] Tsoi W C, James D T, Domingo E B, Kim J S, Al-Hashimi M, Murphy C E, Stingelin N, Heeney M and Kim J-S 2012 Effects of a Heavy Atom on Molecular Order and Morphology in Conjugated Polymer:Fullerene Photovoltaic Blend Thin Films and Devices. *ACS Nano* **6** 9646–56

[85] Casado J, Oliva M M, Deleado M C R, Ortiz R P, Quirante J J, Navarrete J T L, Takimiya K and Otsubo T 2006 Hybrid organic semiconductors including chalcogen atoms in π-conjugated skeletons. Tuning of optical, redox, and vibrational properties by heavy atom conjugation *J. Phys. Chem. A* **110** 7422–30

[86] Reish M E, Nam S, Lee W, Woo H Y and Gordon K C 2012 A Spectroscopic and DFT Study of the Electronic Properties of Carbazole-Based D–A Type Copolymers *J. Phys. Chem. C* **116** 21255–66

[87] Fei Z, Boufflet P, Wood S, Wade J, Moriarty J, Gann E, Ratcliff E L, McNeill C R, Sirringhaus H, Kim J-S and Heeney M 2015 Influence of Backbone Fluorination in Regioregular Poly(3-alkyl-4-fluoro)thiophenes *J. Am. Chem. Soc.* **137** 6866–79

[88] Kim J S, Fei Z, Wood S, James D T, Sim M, Cho K, Heeney M J and Kim J-S 2014 Germanium- and Silicon-Substituted Donor-Acceptor Type Copolymers: Effect of the Bridging Heteroatom on Molecular Packing and Photovoltaic Device Performance *Adv. Energy Mater.* **4** 1400527

[89] Wood S, Kim J-H, Hwang D-H and Kim J-S 2015 Effects of Fluorination and Side Chain Branching on Molecular Conformation and Photovoltaic Performance of Donor–Acceptor Copolymers *Chem. Mater.* **27** 4196–204

[90] Tsoi W C, James D T, Kim J S, Nicholson P G, Murphy C E, Bradley D D C, Nelson J and Kim J-S 2011 The nature of in-plane skeleton Raman modes of P3HT and their correlation to the

degree of molecular order in P3HT:PCBM blend thin films. *J. Am. Chem. Soc.* **133** 9834–43

[91] Gao Y and Grey J K 2009 Resonance chemical imaging of polythiophene/fullerene photovoltaic thin films: mapping morphology-dependent aggregated and unaggregated C=C Species *J. Am. Chem. Soc.* **131** 9654–62

[92] Kim J-H, Song C E, Shin N, Kang H, Wood S, Kang I, Kim B J, Kim B, Kim J, Shin W S and Hwang D-H 2013 High-Crystalline Medium-Band-Gap Polymers Consisting of Benzodithiophene and Benzotriazole Derivatives for Organic Photovoltaic Cells *ACS Appl. Mater. Interfaces* **5** 12820–31

[93] Schmidtke J P, Kim J-S, Gierschner J, Silva C and Friend R H 2007 Optical Spectroscopy of a Polyfluorene Copolymer at High Pressure: Intra- and Intermolecular Interactions *Phys. Rev. Lett.* **99** 167401

[94] Guha S, Graupner W, Resel R, Chandrasekhar M, Chandrasekhar H, Glaser R and Leising G 1999 Planarity of para Hexaphenyl *Phys. Rev. Lett.* **82** 3625–8

[95] Zeng Q G, Ding Z J, Tang X D and Zhang Z M 2005 Pressure effect on photoluminescence and Raman spectra of PPV *J. Lumin.* **115** 32–8

[96] Oberhumer P M, Huang Y-S, Massip S, James D T, Tu G, Albert-Seifried S, Beljonne D, Cornil J, Kim J-S, Huck W T S, Greenham N C, Hodgkiss J M and Friend R H 2011 Tuning the electronic coupling in a low-bandgap donor-acceptor copolymer via the placement of side-chains. *J. Chem. Phys.* **134** 114901

[97] Belton C R, Kanibolotsky A L, Kirkpatrick J, Orofi C, Elmasly S E T, Stavrinou P N, Skabara P J and Bradley D D C 2013 Location , Location , Location - Strategic Positioning of 2 , 1 , 3-Benzothiadiazole Units within Trigonal Quaterfl uorene-Truxene Star-Shaped Structures *Adv. Funct. Mater.* **23** 2792–804

[98] Venkateshvaran D, Nikolka M, Sadhanala A, Lemaur V, Zelazny M, Kepa M, Hurhangee M, Kronemeijer A J, Pecunia V, Nasrallah I, Romanov I, Broch K, McCulloch I, Emin D, Olivier Y, Cornil J, Beljonne D and Sirringhaus H 2014 Approaching disorder-free transport in high-mobility conjugated polymers *Nature* **515** 384–8

[99] Jentzsch T, Juepner H J, Brzezinka K W and Lau A 1998 Efficiency of optical second harmonic generation from pentacene films of different morphology and structure *Thin Solid Films* **315** 273–80

[100] Cheng H-L, Liang X-W, Chou W-Y, Mai Y-S, Yang C-Y, Chang L-R and Tang F-C 2009 Raman spectroscopy applied to reveal polycrystalline grain structures and carrier transport properties of organic semiconductor films: Application to pentacene-based organic transistors *Org. Electron.* **10** 289–98

[101] McNaught A D and Wilkinson A 1997 *IUPAC. Compendium of Chemical Terminology, 2nd ed. (the "Gold Book").* (Oxford: Blackwell Scientific Publications)

[102] Salzillo T, Della Valle R G, Venuti E, Brillante A, Siegrist T, Masino M, Mezzadri F and Girlando A 2016 Two New Polymorphs of the Organic Semiconductor 9,10-Diphenylanthracene: Raman and X-ray Analysis *J. Phys. Chem. C* **120** 1831–40

[103] Brillante A, Valle R G D, Farina L, Girlando A, Masino M and Venuti E 2002 Raman phonon spectra of pentacene polymorphs *Chem. Phys. Lett.* **357** 32–6

[104] Brillante A, Bilotti I, Della Valle R G, Venuti E, Masino M and Girlando A 2005 Characterization of phase purity in organic semiconductors by lattice-phonon confocal Raman mapping: Application to pentacene *Adv. Mater.* **17** 2549–53

[105] Ariu M, Lidzey D and Lavrentiev M 2001 A study of the different structural phases of the polymer poly (9, 9'-dioctyl fluorene) using Raman spectroscopy *Synth. Met.* **116** 217–21

[106] Volz C, Arif M and Guha S 2007 Conformations in dioctyl substituted polyfluorene: A combined theoretical and experimental Raman scattering study *J. Chem. Phys.* **126** 64905

[107] Tsoi W C and Lidzey D G 2008 Raman spectroscopy of fluorene oligomers in the α-, β- and γ-phases *J. Phys. Condens. Matter* **20** 125213

[108] Perevedentsev A, Chander N, Kim J-S and Bradley D D C 2016 Spectroscopic properties of poly(9,9-dioctylfluorene) thin films possessing varied fractions of β-phase chain segments: enhanced photoluminescence efficiency via conformation structuring *J. Polym. Sci. Part B Polym. Phys.* **54** 1995

[109] Brambilla L, Tommasini M, Botiz I, Rahimi K, Agumba J O, Stingelin N and Zerbi G 2014 Regio-Regular Oligo and Poly(3-hexyl thiophene): Precise Structural Markers from the Vibrational Spectra of Oligomer Single Crystals *Macromolecules* **47** 6730–9

[110] Sims M, Tuladhar S M, Nelson J, Maher R C, Campoy-Quiles M, Choulis S A, Mairy M, Bradley D D C, Etchegoin P G, Tregidgo C, Suhling K, Richards D R, Massiot P, Nielsen C B and Steinke J H G 2007 Correlation between microstructure and charge transport in poly(2,5-dimethoxy-p-phenylenevinylene) thin films *Phys. Rev. B* **76** 195206

[111] Chang S S, Tsoi W C, Higgins A M, Kim J-S, Winfield J M and James D T 2010 Self-Assembled, Molecularly Aligned Conjugated Polymer Nanowires via Dewetting *Adv. Funct. Mater.* **20** 3045–54

[112] Kim J-S, Ho P K H, Murphy C E and Friend R H 2004 Phase Separation in Polyfluorene-Based Conjugated Polymer Blends : Lateral and Vertical Analysis of Blend Spin-Cast Thin Films *Macromolecules* **37** 2861–71

[113] Liem H, Etchegoin P, Whitehead K S and Bradley D D C 2002 Raman scattering as a probe of morphology in conjugated polymer thin films *J. Appl. Phys.* **92** 1154–61

[114] Liem H M, Etchegoin P, Whitehead K S and Bradley D D C 2003 Raman anisotropy measurements: An effective probe of molecular orientation in conjugated polymer thin films *Adv. Funct. Mater.* **13** 66–72

[115] Seto K and Furukawa Y 2012 Study on solid structure of pentacene thin films using Raman imaging *J. Raman Spectrosc.* **43** 2015–9

[116] Mino T, Saito Y, Yoshida H, Kawata S and Verma P 2012 Molecular orientation analysis of organic thin films by z-polarization Raman microscope *J. Raman Spectrosc.* **43** 2029–34

[117] James D T, Kjellander B K C, Smaal W T T, Gelinck G H, Combe C, McCulloch I, Wilson R, Burroughes J H, Bradley D D C and Kim J-S 2011 Thin-film morphology of inkjet-printed single-droplet organic transistors using polarized Raman spectroscopy: effect of blending TIPS-pentacene with insulating polymer. *ACS Nano* **5** 9824–35

[118] Onojima N, Nakamura A, Saito H and Daicho N 2015 Aligned growth of TIPS pentacene crystalline domains adhered to Au stripes formed on SiO2 surfaces *J. Cryst. Growth* **432** 146–

51

[119] Wood S, Rigas G-P, Zoladek-Lemanczyk A, Blakesley J C, Georgakopoulos S, Mas-Torrent M, Shkunov M and Castro F A 2016 Precise Characterisation of Molecular Orientation in a Single Crystal Field-Effect Transistor Using Polarised Raman Spectroscopy *Sci. Rep.* **6** 33057

[120] Tsoi W C, Zhang W, Razzell Hollis J, Suh M, Heeney M, McCulloch I and Kim J-S 2013 In-situ monitoring of molecular vibrations of two organic semiconductors in photovoltaic blends and their impact on thin film morphology *Appl. Phys. Lett.* **102** 173302

[121] Wood S, Kim J S, James D T, Tsoi W C, Murphy C E and Kim J-S 2013 Understanding the relationship between molecular order and charge transport properties in conjugated polymer based organic blend photovoltaic devices *J. Chem. Phys.* **139** 64901

[122] Wood S, Garnett O, Tokmoldin N, Tsoi W C, Haque S A and Kim J-S 2014 In situ Formation of Organic-Inorganic Hybrid Nanostructures for Photovoltaic Applications *Faraday Discuss.* **174** 267–79

[123] Yun J-J, Peet J, Cho N-S, Bazan G C, Lee S J and Moskovits M 2008 Insight into the Raman shifts and optical absorption changes upon annealing polymer/fullerene solar cells *Appl. Phys. Lett.* **92** 251912

[124] Wood S, Franklin J B, Stavrinou P N, Mclachlan M A and Kim J-S 2013 Interfacial molecular order of conjugated polymer in P3HT : ZnO bilayer photovoltaics and its impact on device performance *Appl. Phys. Lett.* **103** 153304

[125] Niles E T, Roehling J D, Yamagata H, Wise A J, Spano F C, Moule A J and Grey J K 2012 J-Aggregate Behavior in Poly-3-hexylthiophene Nanofibers *J. Phys. Chem. Lett.* **3** 259–63

[126] Gao J, Stein B W, Thomas A K, Garcia-Galvez J A, Yang J, Kirk M L and Grey J K 2015 Enhanced Charge Transfer Doping Efficiency in J-Aggregate Poly(3-hexylthiophene) Nanofibers *J. Phys. Chem. C* **119** 16396

[127] Wise A J and Grey J K 2012 Resonance Raman studies of excited state structural displacements of conjugated polymers in donor/acceptor charge transfer complexes *Phys. Chem. Chem. Phys.* **14** 11273–6

[128] Gao J and Grey J K 2013 Resonance Raman overtones reveal vibrational displacements and dynamics of crystalline and amorphous poly(3-hexylthiophene) chains in fullerene blends. *J. Chem. Phys.* **139** 44903

[129] Gao J, Thomas A K, Yang J, Aldaz C, Yang G, Qin Y and Grey J K 2015 Polythienylene–Vinylene Structure–Function Correlations Revealed from Resonance Raman Spectroscopy and Photocurrent Imaging *J. Phys. Chem. C* **119** 8980–90

[130] Kelley A M 2013 Resonance Raman overtone intensities and electron-phonon coupling strengths in semiconductor nanocrystals *J. Phys. Chem. A* **117** 6143–9

[131] Jespersen K G, Beenken W J D, Zaushitsyn Y, Yartsev A, Andersson M, Pullerits T and Sundström V 2004 The electronic states of polyfluorene copolymers with alternating donor-acceptor units. *J. Chem. Phys.* **121** 12613–7

[132] Donley C L, Zaumseil J, Andreasen J W, Nielsen M M, Sirringhaus H, Friend R H and Kim J-S 2005 Effects of Packing Structure on the Optoelectronic and Charge Transport Properties in Poly(9,9-di-n-octylfluorene-alt-benzothiadiazole) *J. Am. Chem. Soc.* **127** 12890–9

[133] Martin E J J, Bérubé N, Provencher F, Côté M, Silva C, Doorn S K, Grey J K, Bérubé N, Provencher F, Côté M, Silva C, Doorn S K and Grey J K 2015 Resonance Raman spectroscopy and imaging of push–pull conjugated polymer–fullerene blends *J. Mater. Chem. C* **3** 6058–66

[134] Banerji N, Gagnon E, Morgantini P-Y, Valouch S, Mohebbi A R, Seo J-H, Leclerc M and Heeger A J 2012 Breaking Down the Problem: Optical Transitions, Electronic Structure, and Photoconductivity in Conjugated Polymer PCDTBT and in Its Separate Building Blocks *J. Phys. Chem. C* **116** 11456–69

[135] Karsten B P, Viani L, Gierschner J, Cornil J and Janssen R A J 2009 On the Origin of Small Band Gaps in Alternating Thiophene - Thienopyrazine Oligomers *J. Phys. Chem. A* **113** 10343–50

[136] Mulholland M E, Schwiderski R L, Evenson S J and Rasmussen S C 2012 Molecular Design of Conjugated Materials: Applications of Tunable, Ambipolar, Thieno[3,4-b]pyrazine Building Blocks *Polym. Mater. Sci. Eng.* **107** 36–7

[137] Li W, Hendriks K H, Wienk M M and Janssen R A J 2016 Diketopyrrolopyrrole Polymers for Organic Solar Cells *Acc. Chem. Res.* **49** 78–85

[138] Lucazeau G 2003 Effect of pressure and temperature on Raman spectra of solids: anharmonicity *J. Raman Spectrosc.* **34** 478–96

[139] Jørgensen M, Norrman K and Krebs F C 2008 Stability/degradation of polymer solar cells *Sol. Energy Mater. Sol. Cells* **92** 686–714

[140] Razzell-Hollis J, Tsoi W C and Kim J-S 2013 Directly probing the molecular order of conjugated polymer in OPV blends induced by different film thicknesses, substrates and additives *J. Mater. Chem. C* **1** 6235

[141] Zhao J, Swinnen A, Van Assche G, Manca J, Vanderzande D and Van Mele B 2009 Phase diagram of P3HT/PCBM blends and its implication for the stability of morphology *J. Phys. Chem. B* **113** 1587–91

[142] Clark J, Silva C, Friend R and Spano F 2007 Role of Intermolecular Coupling in the Photophysics of Disordered Organic Semiconductors: Aggregate Emission in Regioregular Polythiophene *Phys. Rev. Lett.* **98** 206406

[143] Reparaz J S, Chavez-Angel E, Wagner M R, Graczykowski B, Gomis-Bresco J, Alzina F and Sotomayor Torres C M 2014 A novel contactless technique for thermal conductivity determination: Two-laser Raman thermometry *Rev. Sci. Instrum.* **85** 34901

[144] Soon Y W, Cho H, Low J, Bronstein H, McCulloch I and Durrant J R 2013 Correlating triplet yield, singlet oxygen generation and photochemical stability in polymer/fullerene blend films *Chem. Commun.* **49** 1291–3

[145] Razzell-Hollis J, Wade J, Tsoi W C, Soon Y, Durrant J and Kim J-S 2014 Photochemical stability of high efficiency PTB7:PC70BM solar cell blends. *J. Mater. Chem. A* **2** 20189–95

[146] Dzwilewski A, Wågberg T and Edman L 2009 Photo-induced and resist-free imprint patterning of fullerene materials for use in functional electronics *J. Am. Chem. Soc.* **131** 4006–11

[147] Li Z, Wong H C, Huang Z, Zhong H, Tan C H, Tsoi W C, Kim J S, Durrant J R and Cabral J T 2013 Performance enhancement of fullerene-based solar cells by light processing *Nat. Commun.* **4** 2227

[148] Yim K-H, Whiting G L, Murphy C E, Halls J J M, Burroughes J H, Friend R H and Kim J-S 2008 Controlling Electrical Properties of Conjugated Polymers via a Solution-Based p-Type Doping *Adv. Mater.* **20** 3319–24

[149] Bruevich V V., Makhmutov T S, Elizarov S G, Nechvolodova E M and Paraschuk D Y 2007 Raman spectroscopy of intermolecular charge transfer complex between a conjugated polymer and an organic acceptor molecule *J. Chem. Phys.* **127** 104905

[150] Bailey J, Wright E N, Wang X, Walker A B, Bradley D D C and Kim J S 2014 Understanding the role of ultra-thin polymeric interlayers in improving efficiency of polymer light emitting diodes *J. Appl. Phys.* **115** 204508

[151] Yamamoto J and Furukawa Y 2016 Raman characterization and electrical properties of poly (3-hexylthiophene) doped electrochemically in an ionic liquid-gated transistor geometry *Org. Electron.* **28** 82–7

[152] Louarn G, Trznadel M, Buisson J P, Laska J, Pron A, Lapkowski M and Lefrant S 1996 Raman Spectroscopic Studies of Regioregular Poly(3-alkylthiophenes) *J. Phys. Chem.* **100** 12532–9

[153] Kim J-S, Ho P K H, Murphy C E, Baynes N and Friend R H 2002 Nature of Non-emissive Black Spots in polymer Light-Emitting Diodes by In-Situ Micro-Raman Spectroscopy *Adv. Mater.* **14** 206–9

[154] Kim J-S, Ho P K H, Murphy C E, Seeley A J A B, Grizzi I, Burroughes J H and Friend R H 2004 Electrical degradation of triarylamine-based light-emitting polymer diodes monitored by micro-Raman spectroscopy *Chem. Phys. Lett.* **386** 2–7

[155] Beatrup D, Wade J, Biniek L, Bronstein H, Hurhangee M, Kim J-S, McCulloch I and Durrant J R 2014 Polaron stability in semiconducting polymer neat films. *Chem. Commun.* **50** 1–4

[156] Wade J, Wood S, Beatrup D, Hurhangee M, Bronstein H, Mcculloch I, Durrant J R and Kim J 2015 Operational electrochemical stability of thiophene-thiazole copolymers probed by resonant Raman spectroscopy Operational electrochemical stability of thiophene-thiazole copolymers probed by resonant Raman spectroscopy *J. Chem. Phys.* **142** 244904

[157] Cheng H L, Chou W Y, Kuo C W, Tang F C and Wang Y W 2006 Electric field-induced structural changes in pentacene-based organic thin-film transistors studied by in situ micro-Raman spectroscopy *Appl. Phys. Lett.* **88** 1–3

[158] Cheng H L L, Chou W Y Y, Kuo C W W, Wang Y W W, Mai Y S S, Tang F C C and Chu S W W 2008 Influence of Electric Field on Microstructures of Pentacene Thin-Films in Field-Effect Transistors *Adv. Funct. Mater.* **18** 285–93

[159] Adil D, Kanimozhi C, Ukah N, Paudel K, Patil S and Guha S 2011 Electrical and optical properties of diketopyrrolopyrrole-based copolymer interfaces in thin film devices *ACS Appl. Mater. Interfaces* **3** 1463–71

[160] Arif M, Guha S, Tsami A and Scherf U 2007 Probing electronic excitations in organic light-emitting diodes via Raman scattering *Appl. Phys. Lett.* **90** 2005–8

[161] Bao Q, Gan Y, Li J and Li C M 2008 Ex and In Situ Confocal Raman Studies of Organic Thin Film and Its On-Working Transistors *J. Phys. Chem. C* **112** 19718–26

[162] Chin X Y, Yin J, Wang Z, Caironi M and Soci C 2014 Mapping polarons in polymer FETs by charge modulation microscopy in the mid-infrared. *Sci. Rep.* **4** 3626

[163] Yin J, Wang Z, Fazzi D, Shen Z and Soci C 2016 First-Principles Study of the Nuclear Dynamics of Doped Conjugated Polymers *J. Phys. Chem. C* **120** 1994–2001

[164] Schlücker S 2014 Surface-enhanced raman spectroscopy: Concepts and chemical applications *Angew. Chemie - Int. Ed.* **53** 4756–95

[165] Blackie E J, Le Ru E C and Etchegoin P G 2009 Single-molecule surface-enhanced raman spectroscopy of nonresonant molecules *J. Am. Chem. Soc.* **131** 14466–72

[166] Kneipp K, Wang Y, Kneipp H, Perelman L T, Itzkan I, Dasari R R and Feld M S 1997 Single molecule detection using surface-enhanced Raman scattering (SERS) *Phys. Rev. Lett.* **78** 1667–1670

[167] Le Ru E C and Etchegoin P G 2012 Single-Molecule Surface-Enhanced Raman Spectroscopy *Annu. Rev. Phys. Chem.* **63** 65–87

[168] Le Ru E and Etchegoin P 2009 *Principles of Surface Enhanced Raman Spectroscopy and Related Plasmonic Effects* (Oxford: Elsevier)

[169] Moskovits M 2005 Surface-enhanced Raman spectroscopy: A brief retrospective *J. Raman Spectrosc.* **36** 485–96

[170] Adil D and Guha S 2012 Surface-Enhanced Raman Spectroscopic Studies of Metal − Semiconductor Interfaces in Organic Field-E ff ect Transistors *J. Phys. Chem. C* **116** 12779–85

[171] Li D, J. Borys N and Lupton J M 2012 Probing the electrode-polymer interface in conjugated polymer devices with surface-enhanced Raman scattering *Appl. Phys. Lett.* **100** 141907

[172] Linde S, Carella A and Shikler R 2012 New approach for analyzing the vertical structure of polymer thin films based on surface-enhanced Raman scattering *Macromolecules* **45** 1476–82

[173] Xu J, Diao Y, Zhou D, Mao Y, Giri G, Chen W, Liu N, Mannsfeld S C B, Xue G and Bao Z 2014 Probing the interfacial molecular packing in TIPS-pentacene organic semiconductors by surface enhanced Raman scattering *J. Mater. Chem. C* **2** 2985–91

[174] Stiles P L, Dieringer J A, Shah N C and Van Duyne R P 2008 Surface-Enhanced Raman Spectroscopy *Annu. Rev. Anal. Chem.* **1** 601–26

[175] Downes A, Mouras R, Mari M and Elfick A 2009 Optimising tip-enhanced optical microscopy *J. Raman Spectrosc.* **40** 1355–60

[176] Kumar N, Mignuzzi S, Su W and Roy D 2015 Tip-enhanced Raman spectroscopy: principles and applications *EPJ Tech. Instrum.* **2** 9

[177] Mauser N and Hartschuh A 2014 Tip-enhanced near-field optical microscopy *Chem. Soc. Rev.* **43** 1248–62

[178] Zhang D, Heinemeyer U, Stanciu C, Sackrow M, Braun K, Hennemann L E, Wang X, Scholz R, Schreiber F and Meixner A J 2010 Nanoscale Spectroscopic Imaging of Organic Semiconductor Films by Plasmon-Polariton Coupling *Phys. Rev. Lett.* **104** 3–6

[179] Wang X, Zhang D, Braun K, Egelhaaf H-J J, Brabec C J and Meixner A J 2010 High-Resolution Spectroscopic Mapping of the Chemical Contrast from Nanometer Domains in P3HT:PCBM Organic Blend Films for Solar-Cell Applications *Adv. Funct. Mater.* **20** 492–9

[180] Camp Jr C H and Cicerone M T 2015 Chemically sensitive bioimaging with coherent Raman

scattering *Nat. Photonics* **9** 295–305

[181] Kukura P, McCamant D W and Mathies R A 2007 Femtosecond stimulated Raman spectroscopy. *Annu. Rev. Phys. Chem.* **58** 461–88

[182] Dietzer D R and Mathies R A 2016 Femtosecond stimulated Raman spectroscopy *Chem. Phys. Chem.* **17** 1224–51

[183] Provencher F, Bérubé N, Parker A W, Greetham G M, Towrie M, Hellmann C, Côté M, Stingelin N, Silva C and Hayes S C 2014 Direct observation of ultrafast long-range charge separation at polymer-fullerene heterojunctions. *Nat. Commun.* **5** 4288